J. Fluid Mech. (2008), *vol.* 597, *pp.* 31–66.
doi:10.1017/S0022112007009718 Printed in the United Kingdom

Streamwise development of turbulent boundary-layer drag reduction with polymer injection

Y. X. HOU, V. S. R. SOMANDEPALLI AND M. G. MUNGAL

Mechanical Engineering Department, Stanford University, Stanford, CA 94305, USA
mungal@stanford.edu

(Received 2 July 2006 and in revised form 2 October 2007)

Zero-pressure-gradient turbulent boundary-layer drag reduction by polymer injection has been studied with particle image velocimetry. Flow fields ranging from low to maximum drag reduction have been investigated. A previously developed technique – the $(1 - y/\delta)$ fit to the total shear stress profile – has been used to evaluate the skin friction, drag reduction and polymer stress. Current results agree well with the semi-log plot of drag reduction *vs.* normalized polymer flux which has been used by previous workers and can be used as a guide to optimize the use of polymer from a single injector. Detailed flow-field statistics show many special features that pertain to polymer flow. It is shown that the mean velocity responds quickly to the suddenly reduced wall shear stress associated with polymer injection. However, it takes a much longer time for the entire Reynolds shear stress profile to adjust to the same change. The Reynolds shear stress profiles in wall units can be higher than unity and this unique feature can be used to further judge whether the flow is in equilibrium. The streamwise evolution of drag reduction magnitude is used to divide the flow into three regions: development region; steady-state region; and depletion region. The polymer stress is estimated and found to be proportional to drag reduction in the depletion region, but not necessarily so in the other regions. The interaction between injected polymer and turbulent activity in a developing boundary-layer flow is dependent upon the flow history and it produces an equally complex relationship between polymer stress and drag reduction. The stress balance in the boundary layer and the dynamical contribution of the various stresses to the total stress are evaluated and it is seen that the polymer stresses can account for up to 25% of the total stress. This finding is in contrast to channel flows with homogeneous polymer injection where the polymer stress is found to account for up to 60% of the total stress.

1. Introduction

The addition of dilute polymer solutions to turbulent wall-bounded flows can cause a significant reduction in the skin friction drag. This drag-reducing effect of polymers, called the Toms effect, has been well known for more than 50 years. This reduction in skin friction, if applied to practical systems optimally, can lead to significant savings in fuel and travel time of ships and submarines. However, there is limited understanding, at present, of the detailed physics behind this phenomenon of drag reduction (DR). The reduction of the skin friction owing to polymer addition causes modification of the mean velocity profile (Virk 1975), changes in the turbulence structure and vorticity in the flow and leads to a redistribution of the stresses in the fluid. This

interaction of the polymer solution with the near-wall turbulence and its subsequent modification of the self-sustaining mechanism of near-wall turbulence (Jimenez & Pinelli 1999) are important to the understanding of the mechanism of polymer DR. Past studies on the physics of DR due to polymers have mainly concentrated on cases with a homogeneous distribution of polymers in a channel or pipe flow, i.e. an ocean of polymer flowing through a channel/pipe. These flow fields are unrealistic in practical external flow applications of polymer DR with wall injection since these application cases involve inhomogeneous polymer concentrations in developing turbulent boundary layers (TBL).

The literature on experimental polymer drag reduction can be broadly separated into: (i) drag reduction in pipes and channels with homogeneous polymer injection; and (ii) drag reduction in boundary layers with inhomogeneous polymer injection. There are many papers about polymer-injected drag reduction in channel/pipe flows, with some notable works being: Warholic, Massah & Hanratty (1999); Warholic *et al.* (2001); Oldaker & Tiederman (1977); Walker, Tiederman & Luchik (1986); and Tiederman, Luchik & Bogard (1985). In contrast to this situation, to our knowledge, there are far fewer major papers on polymer-injected drag reduction in a flat-plate boundary layer, including: Fontaine, Petrie & Brungart (1992); Koskie & Tiederman (1991*a*, *b*); Petrie & Fontaine (1996); Petrie *et al.* (2003); and White, Somandepalli & Mungal (2004). Thus the current study attempts to contribute to a much smaller subset of work in the field of polymer drag reduction – namely that of developing boundary-layer flows with a single point of injection. This flow will naturally bear some similarities to fully developed channel flows, but also some significant differences owing to the depletion of the polymer with downstream distance.

Koskie & Tiederman (1991*b*) used laser-Doppler velocimetry (LDV) to study boundary-layer drag reduction, $Re_\theta = 2478$–3935, with 1000 w.p.p.m. injection, where w.p.p.m. denotes weight parts per million. The polymer concentration at the first measurement position was about 50 w.p.p.m. They concluded that wall shear stress in polymer drag-reduced boundary layers can be determined from velocity measurement in the linear sublayer provided that the near-wall polymer concentration is sufficiently low. The sum of the viscous and Reynolds shear stresses in the polymer drag-reduced boundary layer does not always account for the total shear stress in the region $6 \leqslant y^+ \leqslant 100$. The stress deficit is the polymer stress and will be further discussed below. However, there were no discussions of turbulence statistics profiles and no estimation of polymer stress profiles.

Fontaine *et al.* (1992) provided measurements of concentration profiles and velocity profiles with LDV. The free-stream velocity was 4.5 m s^{-1} and polymer injection concentrations were 500 and 1025 w.p.p.m. An integrated skin friction drag balance plate of a size close to the entire test plate was used to measure the overall integrated drag reduction. No local (at the points where LDV profiles were measured) skin friction was measured or interpolated. As a result, the velocity profiles and statistics profiles were normalized with the no-injection pure water values of the friction velocity and the kinematic viscosity of water. Measured r.m.s. velocity fluctuation profiles and Reynolds shear stress profiles were shown, but are not enough to show systematic trends owing to limited test conditions. There was no estimation and discussion of polymer stress profiles. Petrie *et al.* (2003) studied roughness effects on drag reduction in the boundary layer. The skin friction was also obtained from a large integrated skin friction drag balance plate. A very useful plot, the K plot, was used to relate the amount of polymer-injected and the drag-reduction values. In a TBL, the DR has been observed to be linearly proportional to $\log_{10}(K)$ for a range of K values

and then reach maximum drag reduction (MDR) at larger K values (Vdovin & Smol'yakov 1981; Petrie & Fontaine 1996; Petrie *et al.* 2003). Here, K represents the normalized amount of polymer injected into the flow and will be discussed in detail later. However, there were no discussions of statistics profiles and polymer stress profiles.

White *et al.* (2004) studied drag reduction in a boundary-layer flow using particle image velocimetry (PIV), but only provided measurements at a single axial station far downstream of the injector. Their PIV results, taken in planes parallel to the wall, provided new insights into the flow changes with drag reduction and the resulting streak spacing. In a sense, the present work can be considered a significant extension of this work.

Warholic, Massah & Hanratty (1999) studied homogeneous polymer channel flow (the injected polymer solution was uniformly mixed with the flowing water when it reached the test section, i.e. a homogeneous polymer 'ocean') with LDV measurements. Very good statistics and polymer stress profiles were presented, but there is no streamwise development since the flow was already fully developed. Warholic *et al.* (2001) used PIV to study polymer-injected channel flow. This study presented flow vector fields and a few statistics profiles. Oldaker & Tiederman (1977) studied channel flow with a homogeneous polymer 'ocean'. That study focused on the spatial structure of the sublayer, i.e. streak spacing. Walker *et al.* (1986) studied the optimum combinations of additive concentration, additive flow rate, injector angle, and injector width in channel flow. The studies of McComb & Rabie (1982) in pipe flow and Tiederman *et al.* (1985) in channel flow showed that the polymer action is confined close to the wall. There were no discussions of statistics profiles in Tiederman *et al.* (1985), Walker *et al.* (1986) and Oldaker & Tiederman (1977).

It is important to note that some flow behaviours in the boundary layer are similar to channel flows (e.g. changes in mean profiles, changes in Reynolds stress). However, there are key differences associated with the downstream development of these quantities and their response to the injection of the polymer which is the subject of the current work. In fact, it is the complicated development of the flow field that makes the boundary-layer problem interesting and challenging.

The behaviour of a passive contaminant dye injected into a TBL has been described by Poreh & Cermak (1964) and Fontaine *et al.* (1992) and is briefly repeated here. The dye concentration layer goes through initial, intermediate, transition and final diffusion zones from upstream to downstream. A diffusion boundary-layer thickness, λ, was defined as the distance from the wall at which the mean concentration drops to 50% of its maximum. The values of λ/δ in different zones are about: <0.1 in the initial zone; 0.1–0.39 in the intermediate zone, 0.39–0.64 in the transition zone; and almost constant at 0.64 in the final zone. The lengths of the first three zones are such that: the initial zone is very thin and short; the intermediate zone is about $18\delta_{av}$; and the transition zone is about $60\delta_{av}$, where δ_{av} is the average boundary-layer thickness from the upstream line source to the location considered. It is also well known that polymer dispersion in a TBL is significantly different from that of a passive dye. Polymer modifies the turbulence and is better described as active, rather than passive. The polymer diffuses at a slower rate than that of a passive contaminant and the initial zone is lengthened relative to that of a passive contaminant (Fruman & Tulin 1976; Latto & El Reidy 1976; Vdovin & Smol'yakov 1978, 1981; Walker & Tiederman 1988, 1989, 1990; Brungart *et al.* 1991; Fontaine *et al.* 1992). These results also showed that much of the initial zone is a region of near-MDR owing to the high concentration of polymer. Although it is clear that the diffusion of

polymer and passive contaminants are different, it is reasonable to expect that the polymer diffusion and the DR will go through three similar regions from upstream to downstream based on the DR values: development region (consisting of initial and intermediate regions); steady-state region; and depletion region. It is expected that DR increases quickly in the development region as the polymer starts to be effective, then remains relatively constant in the steady-state region and finally reduces in the depletion region.

One important quantity to be determined in the study of DR is the wall shear stress. The total shear stress in the Newtonian zero pressure gradient (ZPG) TBL is the sum of the viscous and Reynolds shear stresses. In the polymer DR TBL, the total shear stress (τ_{total}) is composed of three quantities: viscous stress ($\mu\partial u/\partial y$); Reynolds shear stress ($\rho(-\overline{u'v'})$); and polymer stress (τ_p). Equation (1) is used to calculate the total shear stress in dilute polymer flow (Min *et al.* 2003),

$$\tau_{total} = \tau_p + \mu\partial u/\partial y + \rho(-\overline{u'v'}), \tag{1}$$

where, μ is the solution viscosity, u is the mean streamwise velocity, y is the axis normal to the flat plate, ρ is the solution density, and u' and v' are streamwise and vertical (normal to the wall) velocity fluctuations.

Both $\partial u/\partial y$ and $-\overline{u'v'}$ in (1) can be measured or evaluated directly, but not the polymer stress τ_p. In a polymer drag-reduced flow, the 'stress deficit' phenomenon is noticed in equilibrium flows (such as channel flows), where the sum of turbulent and viscous terms does not give the expected linear distribution of the total stress. There is a 'stress deficit' if the $[\mu\partial u/\partial y + \rho(-\overline{u'v'})]$ profile is compared to the total shear stress profile owing to the missing (i.e. unmeasured) polymer stress (Koskie & Tiederman 1991*b*; Warholic *et al.* 1999). It is this additional polymer stress which makes it difficult to evaluate the wall shear stress. White *et al.* (2006) extended the analysis of the dynamical contributions to the skin-friction in channel flow by Fukagata, Iwamoto & Kasagi (2002) to ZPG TBL with Newtonian fluid or dilute polymer solution, where the viscosity is roughly constant. The TBL streamwise momentum equation was integrated three times in the wall-normal direction. The force balance, the mean velocity profile and the mass flow rate were obtained by the first, second and third integrations, respectively. Manipulating terms after the third integration yielded,

$$C_f \equiv \tau_w/\left(\tfrac{1}{2}\rho U^2\right) = \underbrace{\frac{4(1-\delta^*)}{\mathrm{Re}_\delta}}_{\mathrm{I}} + \underbrace{2\int_0^1 2(1-y^*)(-\overline{u'v'}^*)\mathrm{d}y^*}_{\mathrm{II}}$$
$$+ \underbrace{2\int_0^1 (1-y^*)^2\left(-\frac{\partial\bar{\tau}}{\partial y^*}\right)\mathrm{d}y^*}_{\mathrm{III}} + \underbrace{2\int_0^1 2(1-y^*)\bar{\tau}_p\mathrm{d}y^*}_{\mathrm{IV}}, \tag{2}$$

where, C_f is the skin friction coefficient, τ_w is the wall shear stress, U is the free-stream velocity, Re_δ is the Reynolds number based on the boundary-layer thickness δ(taken to be the boundary-layer thickness at $u/U = 99\%$ in this work), δ^* is the displacement thickness normalized by δ, y^* is the wall normal coordinate normalized by δ, $-\overline{u'v'}^*$ is the Reynolds shear stress normalized by U^2, $\bar{\tau}_p$ is the polymer stress normalized by ρU^2 for a polymer solution ($\bar{\tau}_p = 0$ for Newtonian fluid) and $\bar{\tau}$ is the total shear stress

normalized by ρU^2. Equation (2) shows that the wall shear stress is determined by the sum of four terms: viscous term (I), Reynolds stress (II), total stress gradient (III) and polymer stress (IV). The sum of these four terms, determines the skin friction with, possibly, a non-unique combination of them for a given value of skin friction coefficient.

Inspired by this analysis, Hou, Somandepalli & Mungal (2006) developed a technique, based upon $(1 - y/\delta)$ fitting, to determine the wall shear stress and used it to obtain the polymer stress profile. The same technique has been applied in this study. Furthermore, the profile of the polymer stress and its relation to the observed DR are important for understanding the interaction between the polymer and the turbulence. Intuitively, we might guess that the polymer stress is proportional to the DR, i.e. the larger the polymer stress, the higher the DR value. However, the polymer stress has not been studied extensively so the present study will also report on the polymer stress development.

Parallel to experimental studies, there are many studies of polymer DR flows via simulations (e.g. den Toonder *et al.* 1997; Dimitropoulos, Sureshkumar & Beris 1998; Dimitropoulos *et al.* 2001; Sibilla & Baron 2002; Min *et al.* 2003; Dubief *et al.* 2004; Terrapon *et al.* 2004; Paschkewitz *et al.* 2005). Such numerical simulations can provide more details of the flow field than experimental studies. However, modelling of the polymer dynamics is typically required in these simulations and hence experimental results are required for the purpose of comparison and validation of these models.

As outlined above, in the literature, there are relatively few studies in TBL DR with polymer injection. There have been many studies in channel (and pipe) flows. The study of channel flow was often considered as a substitute for boundary-layer flows, but this can be misleading to some degree since the boundary-layer flow is continuously evolving as the polymer close to the wall is continuously depleting. The existing studies of boundary-layer DR do not fully answer many questions that are important and special for TBL DR flows. This paper attempts to study DR in a TBL systematically, using PIV to obtain velocity and turbulence statistics data and provide information that was not obtained in previous studies. Various concentrations of polymer solution are injected into a ZPG TBL and the DR is studied at various streamwise locations. The data presented here provide a quantitative measure of the polymer effects on near-wall turbulence. The data can also be used to validate models for simulating polymer DR and can help in formulating new models that capture the physics of inhomogeneous polymer DR better. In summary, this work attempts to address the following issues.

1. What is the streamwise development of the mean velocity profiles, r.m.s. velocity profiles and Reynolds stress profiles in a drag-reduced flow?
2. What is the polymer stress? How is it distributed across the boundary layer and what is its streamwise development?
3. Which flow parameters respond most quickly to the injection effect and how?
4. Is the flow in a state of equilibrium as it evolves downstream?
5. Is the polymer stress proportional to the drag reduction?
6. What is the contribution of the polymer stress to the total skin friction?
7. How does the drag reduction observed relate to the injection concentration and distance from injection?
8. How to provide detailed and systematic data on polymer drag reduction in lower-Reynolds-number flow to benchmark DNS and LES results.

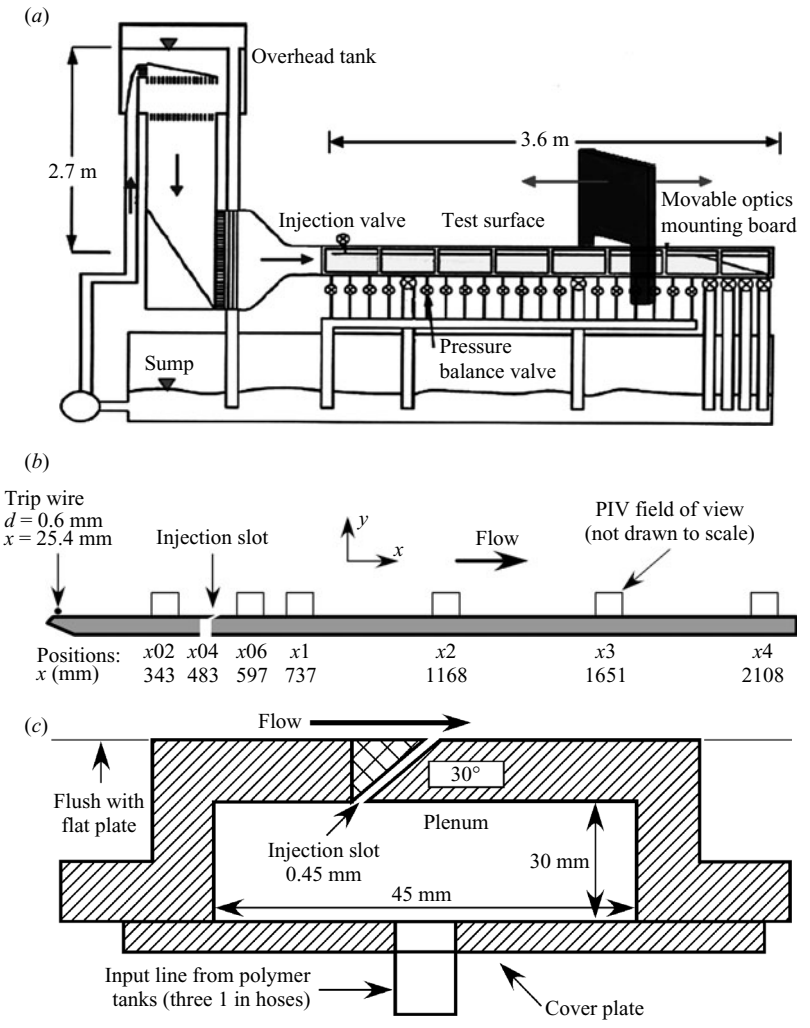

FIGURE 1. Experiment facility: (*a*) closed loop water tunnel; (*b*) flat plate showing measurement positions; (*c*) details of injection slot.

2. Experimental set-up

The experiments were conducted in a constant-head closed-circuit water tunnel figure 1(*a*). The boundary-layer test surface was the upper wall of the test section of the tunnel. Manual valves located on the lower surface and the sidewalls of the tunnel were adjusted to maintain a ZPG condition along the top wall. The test section had a cross-section of 0.36 m in span and 0.13 m in height with a length of 3.66 m. The walls of the tunnel were constructed from acrylic to provide full optical access. The inlet velocity could be varied from 0.3 to 0.7 m s^{-1}; however, for all experiments reported in this paper, the inlet velocity was maintained constant at 0.5 m s^{-1}. The water in the closed-circuit tunnel was maintained at a constant temperature of 18°C using a refrigerated chiller which maintains the water temperature to within 0.2° of the set value. The leading edge of the test wall was a half-ellipse with major to minor axis ratio of 16. A 0.6 mm diameter rod glued 25.4 mm downstream of the leading edge was used to trip the boundary layer and make it turbulent. A detailed

Typical TBL parameters for $U = 0.5$ m s^{-1}

Position	x (mm)	x^+ (based on local u_τ)	δ (mm)	θ (mm)	Re_θ
$x02$	343	7690	13	1.6	730
Injection slot 0.45 mm at 30°	483	10 640	15	1.8	840
$x06$	597	12 900	17	2.1	970
$x1$	737	15 320	20	2.5	1150
$x2$	1168	23 320	27	3.5	1620
$x3$	1651	31 310	35	4.5	2060
$x4$	2108	39 400	41	5.2	2380

TABLE 1. Newtonian TBL parameters. x = distance from leading edge; δ = boundary-layer thickness at $u/U = 99\%$; θ = momentum thickness, and Re_θ = Reynolds number based on momentum thickness = $U\,\theta/\nu$.

description of the water-tunnel facility is given in White *et al.* (2004). At the start of an experiment, the tunnel was carefully filled with water to avoid entrapment of air on the test wall and inside the tunnel. Any residual air was removed by running the tunnel for several hours before any measurements were taken. Once all air was removed and the water temperature had stabilized, the required velocity was set and a ZPG was achieved along the tunnel by adjusting the manual bleed valves on the lower and side walls of the tunnel. The ZPG condition was verified by obtaining multiple velocity measurements at several streamwise locations along the tunnel and ensuring that $\mathrm{d}u/\mathrm{d}x = 0$ along the length of the tunnel.

Figure 1(*b*) shows a schematic of the top-wall flat plate on which the boundary layer developed for the present experiments. There are six measurement positions on the flat plate labelled $x02$, $x06$, $x1$, $x2$, $x3$ and $x4$. Also shown is the injection slot that was located between position $x02$ and $x06$ and was 483 mm downstream of the plate's leading edge. For a purely Newtonian boundary layer with a free-stream velocity of 0.5 m s^{-1}, the boundary-layer thickness varied from 13 mm at position $x02$ to 42 mm at position $x4$. Table 1 gives a comprehensive listing of the boundary-layer parameters at each of the measurement locations.

2.1. *PIV details*

PIV was used to measure velocity and velocity statistics in these experiments. The PIV system used a Peltier cooled 12 bit CCD camera with a resolution of 1280 × 1024 pixels, a dual-head pulsed Nd:YAG laser operating at 532 nm, and appropriate sheet forming optics. A 532 nm narrowband filter was used in conjunction with the camera optics to allow only the laser light scattered by the tracer particles into the camera. The flow was naturally seeded with residual dust particles in the water of size less than 10 μm. All particles above this size had been removed by a series of filters before the water entered the tunnel system. Many types of seeding particles have been tested and none of them gave better images than those obtained from natural seeding. The natural seeding gave consistent and very good particle images so that natural seeding was then the best and simplest choice for the PIV measurement. The PIV processing used a multi-pass iterative scheme starting with a cross-correlation window box size of 64 × 64 pixels and a final pass at 32 × 32 pixels with 50% overlap between adjacent correlation regions. The spatial resolution of the camera was 13.6 μm per pixel with an effective field of view of 17.4 mm × 13.9 mm. The smallest scale resolved was 435 μm. At a fixed streamwise location, PIV images were

obtained across the full thickness of the boundary layer in the (x, y) -plane (the plane perpendicular to the flat plate and in line with the flow direction). Closer to the leading edge, a single PIV image spanned the entire thickness of the boundary layer; while further downstream, as the thickness of the boundary layer increased, multiple PIV images in the wall normal direction were required to span the entire thickness of the boundary layer. One thousand image pairs were acquired at each streamwise location. Since there are 32 vectors in each PIV vector field at the same wall normal location (i.e. same y value), they are streamwise averaged. The final boundary profiles are the combination of time and space averages with 32 000 vectors for each data point (1000 in time $\times$ 32 in space).

2.2. *Polymer solution preparation and injection*

The polymers used in the DR experiments were polyethylene oxide (PEO) with brand name POLYOX^{TM}WSR-Coagulant ('COA') and WSR-301 ('301') from Dow Chemical. The mean molecular weights, based on the manufacturer's specification sheet, were $\sim$5 million and $\sim$4 million for COA and 301, respectively. The viscosity (mPaS) for 1% weight mixed with glycol were given by the manufacturer as 5500–7500 and 1650–5500 for COA and 301, respectively. The polymer solution in the current study avoided the use of glycol and was prepared by directly mixing the polymer powder with water. The precisely weighed polymer powder was slowly shaken into solution with water in a container using a water shower head sprayer. The water was filtered by a carbon filter to remove all contaminants and residual chlorine. After all polymer powder had been added to the solution, it was gently stirred for several hours periodically. The solutions were then allowed to stand for at least 20 h to homogenize and allow degassing.

The polymer solution was injected into the boundary layer through an injection slot by pressurizing its holding container slightly above the tunnel pressure ($\sim$41 kPa) with compressed air. The dimensions of the injection slot were 0.45 mm in height, 310 mm in span, 10 mm long in the polymer solution flow direction, and it was inclined at 30° to the flat plate (figure 1*c*). Note that this left a 25 mm gap on each side between the injector and the sidewall. Although the injector was not full span, flow-visualization measurements were conducted to prove that the centreline of the flat plate, where the measurements were conducted, was still fully two-dimensional and free of any effect from the two gaps. A small plenum chamber of 320 mm by 45 mm by 30 mm, located above the injection slot, was used to equilibrate pressure and provide uniform flow across the span of the injection slot. The flow rate of the injected polymer solution was measured by monitoring the compressed air flow rate with a commercially available flow meter. The injector was located 483 mm downstream of the flat plate's leading edge.

The injection rate of polymer is denoted by the ratio Q_i/Q_s, where Q_i is the flow rate of the injected fluid per unit width; Q_s ($= 67.3\nu$, where ν is the kinematic viscosity of water with value of 1.0554×10^6 m^2 s^{-1} at 18 °C) is the volume flow rate per unit width of water in the viscous sublayer (defined by the sublayer edge at $y^+ = 11.6$) of the boundary layer and is independent of velocity. In order to minimize the disturbance of the injected flow on the boundary layer, Q_i should be smaller or of the same order as Q_s (Wu & Tulin 1972; Walker *et al.* 1986; Fontaine *et al.* 1992). The typical injection rate in the current experiment was about 0.77 so that the injection disturbance was small. The parameters of the injector with typical injection rate of 0.77 are shown in table 2. It shows that the injector width in plus units is 11 and is within the sublayer. The injection velocity is high at 23% of the free-stream velocity.

L (mm) (injector width)	0.45
x (mm) (from leading edge)	483
δ (mm) at injector	15
u_τ (m s^{-1}) at injector	0.024
u_{inj} (m s^{-1}) (through injector)	0.115
L^+	11
u_{inj}/U	0.23

TABLE 2. Parameters of the injector with typical injection rate of $Q_i/Q_s = 0.77$.

However, as shown below, the overall disturbance to the flow owing to injection is quite small and can be neglected.

2.3. *Effect of injection scheme on TBL*

Figure 2 compares the mean velocity profiles and Reynolds shear stress profiles with and without water injection. The injection disturbance effect is so small that there is essentially no difference in the mean velocity profiles in water injected and non-injected flows. There is some small initial difference in the Reynolds shear stress profiles, as shown in figure 2(b) at position $x06$, but the difference disappears further downstream at positions $x2$ and $x4$. These results prove that the change in the boundary-layer flow owing to water injection is negligible and any changes seen in polymer injected flows are due to the effect of the injected polymer and not the injection process itself. To further validate the quality of the ZPG TBL facility and the PIV measurement technique, the current u_{rms} data and Reynolds shear stress data are compared with those in Fernholz & Finley (1996) (figure 3). The data are measured from figures in Fernholz & Finley (1996), who plotted the data from Purtell, Klebanoff & Buckley (1981), Erm (1988), Roach & Brieley (1989), Brasseur (1994 personal communication to Fernholz & Finley), and Warnack (1994 personal communication to Fernholz & Finley). A detailed description of the data can be found in their paper and is not repeated here. As shown in figure 3(a), the current u_{rms} agrees very well with that from other sources for $y^+ > 10$. The current PIV measurement could not resolve u_{rms} correctly for $y^+ < 10$ and this is expected since the PIV measurement was not optimized for sublayer measurement. Furthermore, it is clear that there is no difference in u_{rms} between water-injected flow and the corresponding non-injected flow. Figure 3(b) shows excellent agreement between the current Reynolds shear stress profiles and those from other sources. The current Reynolds shear stresses at position $x06$ ($Re_\theta = 970$), position $x1$ ($Re_\theta = 1620$) and position $x4$ ($Re_\theta = 2380$) agree well with other data of $Re_\theta = 984$, $Re_\theta = 1567$ and $Re_\theta = 2244$, respectively. The good agreement of the current u_{rms} and Reynolds shear stress with those from several other sources confirms the high quality of the ZPG TBL facility and the overall accuracy of the PIV system.

2.4. *Data reduction*

There are several ways to define the DR value. In this study, it is defined by

$$DR = 100 \times (\tau_{water} - \tau_{polymer})/\tau_{water}, \tag{3}$$

where $\tau_{polymer}$ and τ_{water} are the skin friction (wall shear stress) of polymer flow and the corresponding Newtonian flow, respectively.

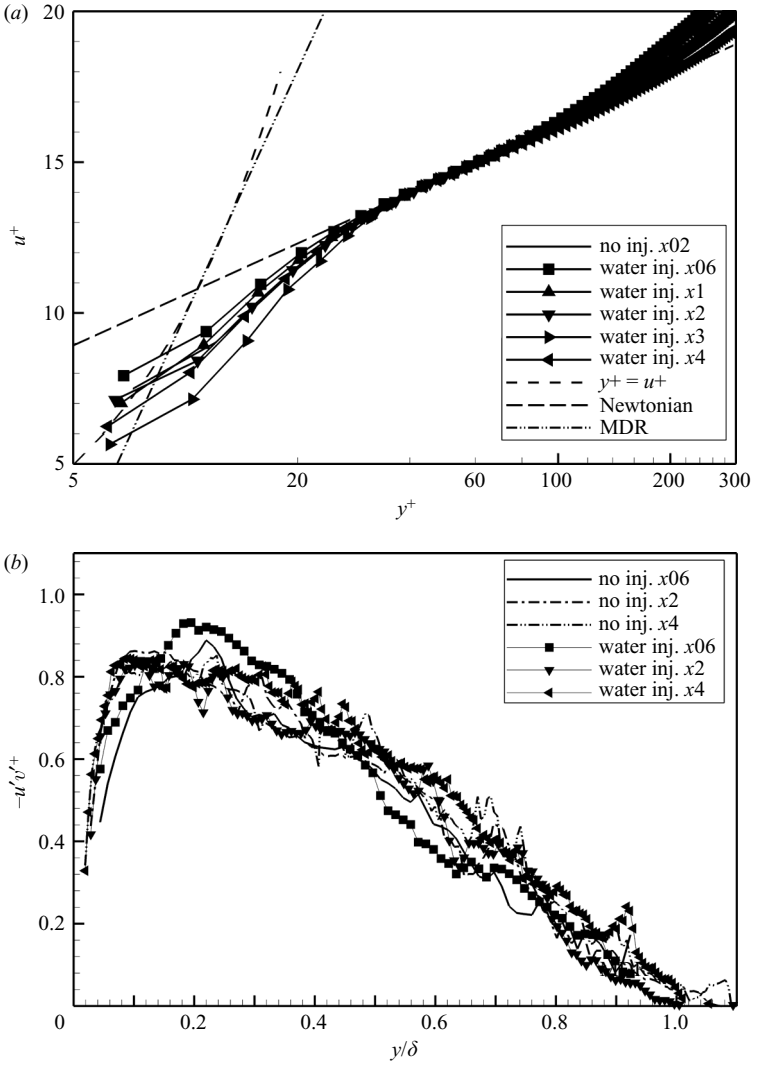

FIGURE 2. Disturbance effects of water injection.

2.4.1. *Computing skin friction*

An important parameter to be measured in the current study is the skin friction for both Newtonian flow and polymer (injected) flow. There are many ways to obtain the skin friction for Newtonian flow, i.e. shear stress sensors or evaluation from the mean velocity profile by using the Clauser chart. The second method, the Clauser chart, is used in the current study for Newtonian flow. The skin friction of polymer flow, however, is problematic since evaluation from the mean velocity profile by the Clauser chart does not work. Hou *et al.* (2006) solved this problem by using a $(1 - y/\delta)$ fit to the total shear stress profile to obtain the wall shear stress. The same fit is used here with the PIV data to estimate the skin friction and DR. Sometimes, however, the flow close to the injection slot is in the process of adjusting to the effect of injected

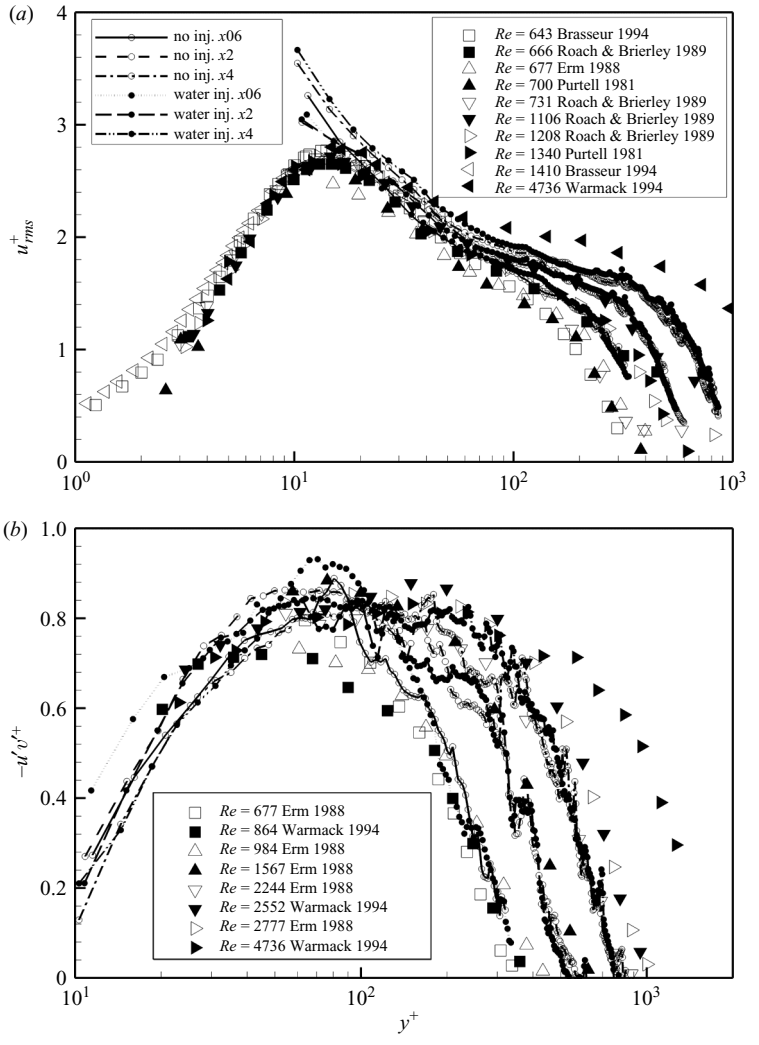

FIGURE 3. Comparison of current flow fields with those in Fernholz & Finley (1996). (*a*) u_{rms} measured from figures 14 and 15 in Fernholz & Finley (1996); (*b*) Reynolds shear stress measured from figure 24 in Fernholz & Finley (1996). The line styles in (*a*) and (*b*) are the same.

polymer and, hence, is not in equilibrium and the $(1 - y/\delta)$ fit fails to work in this region of flow adjustment. The value of DR in such a situation is estimated from the mean velocity profile slope. The slope of the mean velocity profile in DR flow, when plotted in semi-log format, increases with the value of DR (e.g. see figures 3 and 10 of Warholic *et al.* 1999). When the $(1 - y/\delta)$ approach failed in the situations where the flow is not in equilibrium, the measured mean velocity profile is compared with those where the DR values are known and the wall shear stress estimated. The uncertainty of the wall shear stress obtained from the mean velocity profile is relatively higher than that obtained from the $(1-y/\delta)$ fit. Nevertheless, the uncertainty of the estimated DR value is within 10%. If the DR value, as estimated, is too far away from its true value, i.e. more than 10%, the normalized flow parameters show an unusual distribution that warn us to double check the estimation.

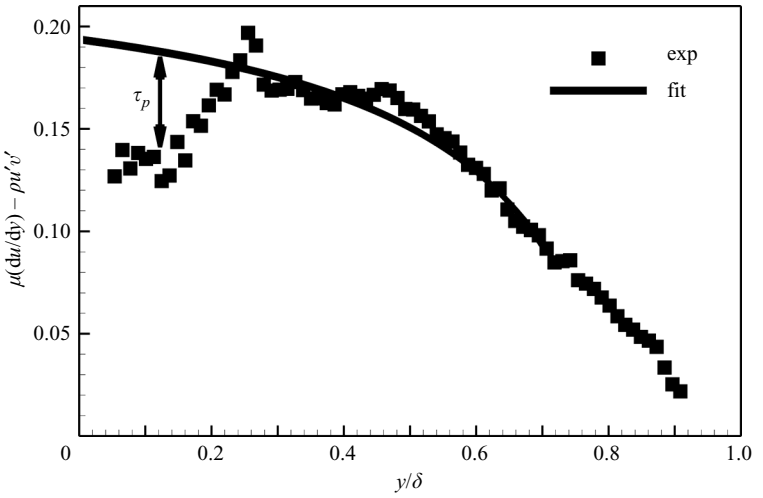

FIGURE 4. Shear stress in polymer injected flow. (Note: the $(1 - y/\delta)$ fit is done within $0.3 < y/\delta < 0.7$)

2.4.2. *Polymer stress estimation*

As stated in §1, in the polymer DR TBL, there is a 'stress deficit' if the $[\mu\partial u/\partial y + \rho(-\overline{u'v'})]$ profile is compared to the total shear stress profile, with the missing part being the polymer stress. Figure 4 shows a typical $[\mu\partial u/\partial y + \rho(-\overline{u'v'})]$ profile in polymer DR flow along with the best fit obtained from the $(1-y/\delta)$ method. It is clearly seen that there is a 'stress deficit' associated with the polymer stress, as indicated by the arrow, equal to the difference between the measured total stress and the fitted stress. A full justification of the validity of this approach is given in Hou *et al.* (2006).

3. Streamwise development of drag reduction

The DR values for different injection conditions are shown in tables 3 and 4 and plotted in figure 5. MDR is obtained for polymer injection concentrations (C_i) of 1000 and 2000 w.p.p.m. Results show that, in these cases, the development region is very short and not detectable. The steady-state region is long for $C_i \geqslant 500$ w.p.p.m. The depletion region is observed for $C_i = 250$ and 100 w.p.p.m. The steady-state region here is based solely on the DR values. As will become clear later, the flow may not be in equilibrium when it is in the steady-state region (constant DR values), i.e. position $x2$ to $x4$ for 301 with $C_i = 2000$ w.p.p.m. The non-equilibrium flow, which starts as soon as the polymer is injected, may end within the development region, or steady-state region. Furthermore, the flow at MDR is not necessarily at equilibrium. The three DR regions defined here are based only on the DR values and the same DR values can be achieved via many different flow conditions, i.e. equilibrium or otherwise. This non-unique path to reach a DR value (or a skin friction value) will become clearer later when the dynamical contributions to the skin-friction analysis (White *et al.* 2006) is discussed.

The streamwise development of DR is different for COA and 301 at $C_i = 500$ w.p.p.m. The DR for COA starts with high and nearly constant values and then reduces at downstream positions $x3$ and $x4$, whereas the DR value for 301 starts relatively low at the upstream locations and increases further downstream. The

	DR of PEO WSR-coagulant					
Conc. w.p.p.m.	2000	1000	1000	500	250	100
Q_i/Q_s	0.77	1.1	0.77	0.82	0.79	0.79
$x06$	75	74	72	60	50	32
$x1$	78	72	72	60	50	32
$x2$	78	70	72	62	48	15
$x3$	77	66	72	43	37	5
$x4$	70	60	62	35	20	8

TABLE 3. Drag reduction of PEO WSR-coagulant.

	DR of PEO WSR-301				
Conc. w.p.p.m.	2000	1000	500	250	100
Qi/Qs	0.75	0.77	0.79	0.82	0.78
$x06$	77	75	45	40	35
$x1$	79	75	50	54	45
$x2$	77	70	69	38	34
$x3$	76	71	61	38	10
$x4$	76	65	64	18	15

TABLE 4. Drag reduction of PEO WSR-301.

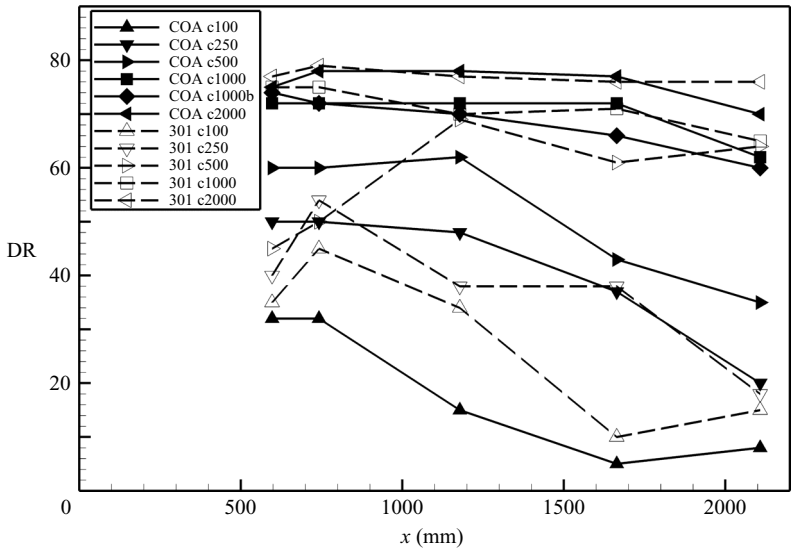

FIGURE 5. Streamwise development of drag reduction.

different trends can be explained by the different DR regions. COA may have a much shorter development region such that it is already in the steady-state region at position $x06$ and enters the depletion region around position $x3$. Contrary to COA, 301 is still in the development region until position $x1$ and then enters the steady-state region at position $x2$. The trends of DR values are similar for both COA and 301 at $C_i = 250$ w.p.p.m. Both flows start with relatively high DR and reduce at downstream locations. Similarly, the DR in $C_i = 100$ w.p.p.m. flow reduces from upstream to downstream except at the last position $x4$, where the estimated DR is

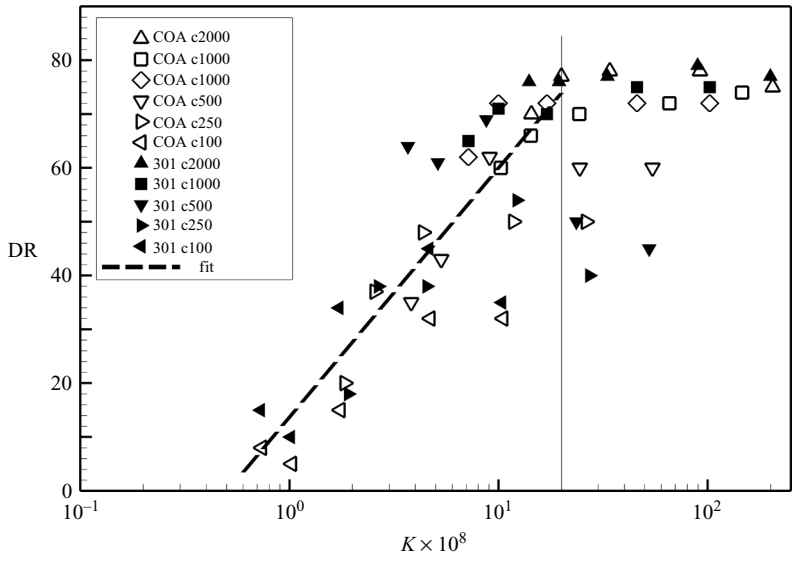

FIGURE 6. Drag reduction *vs.* K. The dashed line is a linear fit to the data at the left of the vertical line ($K \leqslant 2 \times 10^{-7}$) with equation: $\mathrm{DR} = 46.3 \log_{10}(K \times 10^8) + 13.7$.

higher than that at position $x3$. The most likely reason is some background polymer accumulation. The water tunnel is a closed loop tunnel and the injected polymer may not be completely destroyed by the pump and accumulates as a background concentration. When the data at position $x4$ was being taken, a small part of the polymer that had been injected into the tunnel for positions $x06$ to $x3$ accumulated in the water and reached a concentration that was high enough to cause additional DR (Warholic *et al.* 1999). This effect was noticeable for only $C_i = 100$ w.p.p.m. mainly because the background effect is not large and, hence, does not cause any significant difference in the DR for higher concentration injections. Nevertheless, the rebound is only 5% and is within the uncertainty of the DR evaluation and could also be an artefact of the DR evaluation – further comments will be made on this point later.

As stated in §1, the plot of DR *vs.* $\log_{10}(K)$ had been used (Vdovin & Smol'yakov 1981; Petrie & Fontaine 1996; Petrie *et al.* 2003) to collapse experimental data, where $K = (QC_m)/(\rho U X_S)$, Q is the volume flux of injected polymer solution per unit span, C_m is the mass concentration of polymer solution (i.e. kg m^{-3}), ρ is the water density, U is the free-stream velocity, and X_S is the downstream measurement location. The current data, plotted in the same format, are shown in figure 6. As seen, the DR value increases almost linearly with $\log_{10}(K)$ for K from 10^{-8} to 20×10^{-8}. The DR value is constant at MDR for K greater than 20×10^{-8}. Any extra polymer added above this limit, i.e. K greater than 20×10^{-8}, is apparently wasted. The plot of DR *vs.* $\log_{10}(K)$ can be used as a guide to optimize the use of polymer for single slots, i.e. estimating the minimum amount of polymer required to sustain high DR. The DR *vs.* $\log_{10}(K)$ is further discussed later.

4. Velocity profiles and statistics

4.1. *Mean velocity profiles*

Selected mean velocity profiles, u/U *vs.* y/δ, are shown in figure 7. There is a significant difference between polymer flows and the corresponding Newtonian flows.

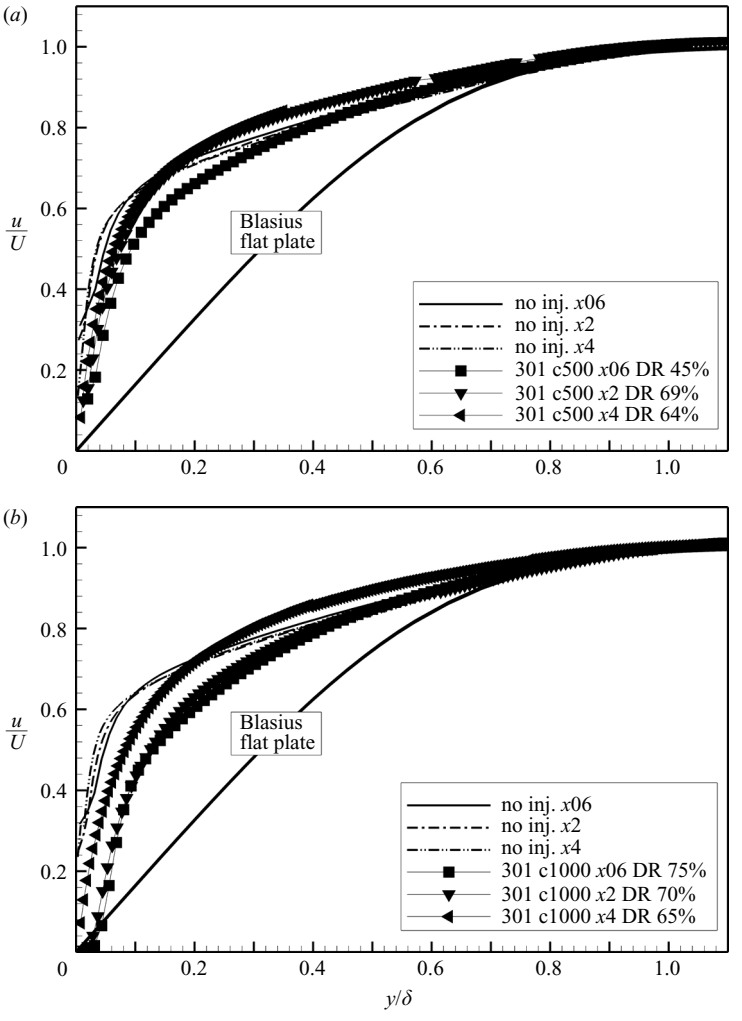

FIGURE 7. Mean streamwise velocity profiles in outer coordinates.

The polymer flow profiles all lie between that of Newtonian turbulent flow and laminar (Blasius) flow, however, the polymer flow is much closer to the Newtonian turbulent flow and well away from the laminar flow. The near-wall velocity gradient, $\mathrm{d}u/\mathrm{d}y$, is smaller in polymer flows and reflects the fact that the skin friction, in these cases, is smaller than that of the corresponding Newtonian flow. The velocity of polymer flow is smaller than that of the Newtonian flow in the lower part of the boundary layer, i.e. $y/\delta < 0.1 - 0.2$. Further away from the wall, the Newtonian velocity profiles and polymer DR velocity profiles cross over and attain the same free-stream velocity with the same boundary-layer thickness δ.

Figure 8 shows u^+ *vs.* y^+ at different streamwise positions for 301 with $C_i = 100$, 250, 500, 1000 and 2000 w.p.p.m. Three reference lines are also shown in the figure: the linear sublayer, $u^+ = y^+$; the classical incompressible Newtonian ZPG TBL log law; and the Virk (1975) MDR profile. The latter two lines are obtained from the same equation, $u^+ = (1/k)\ln(y^+) + B$, with different k and B values: the values for Newtonian flow are $k = 0.40$ and $B = 5.10$, while the values for MDR are $k = 11.7$

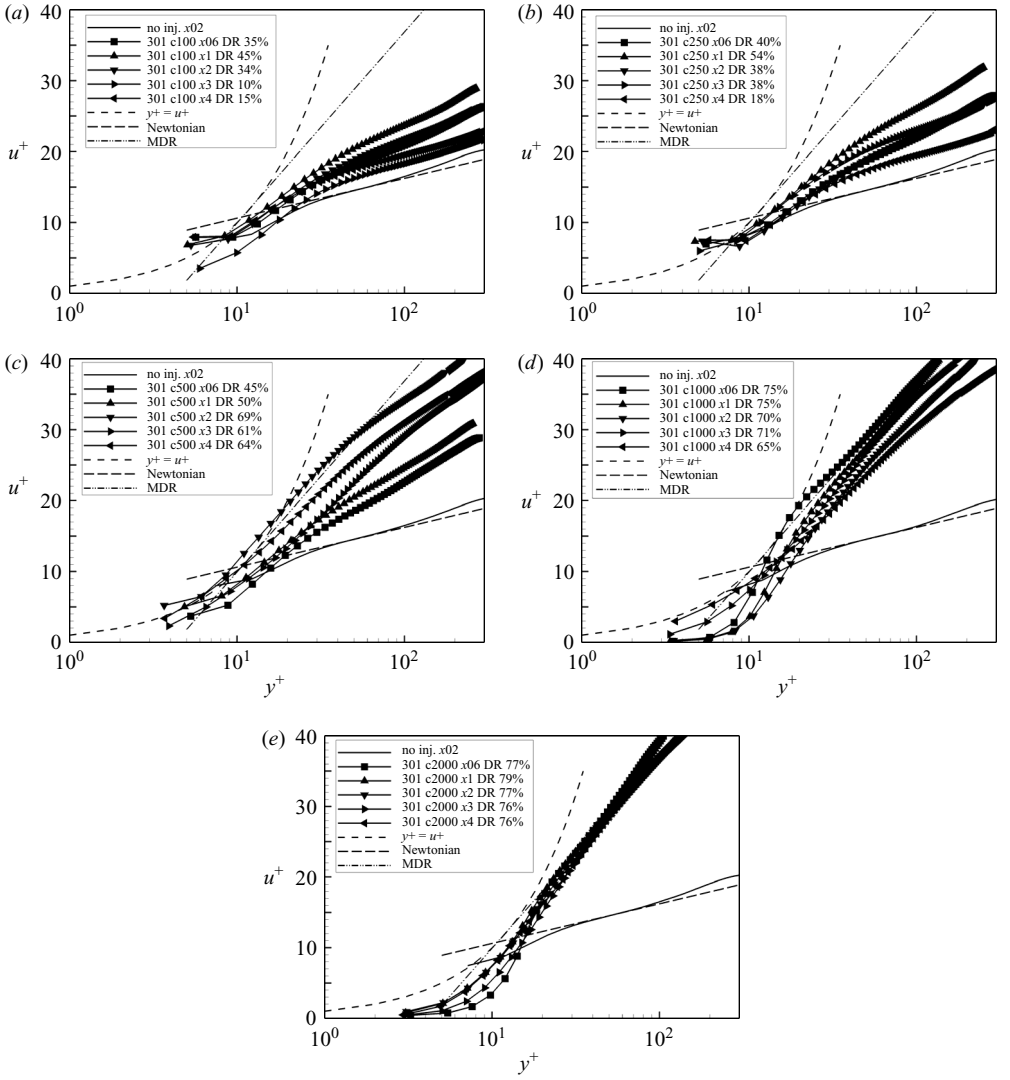

FIGURE 8. Mean streamwise velocity in wall units.

and $B = -17$. These two lines serve as the lower and upper bounds for the actual DR flows. When the DR is low, i.e. positions $x3$ and $x4$ shown in figure 8(a), the mean velocity profiles have the same slopes as that of the classical incompressible ZPG TBL profile, but are shifted upward. When the DR is higher, i.e. position $x06$, $x1$ and $x2$ in figure 8(a), the profiles are not only shifted upward but also have higher slopes than that of the ZPG TBL. The slope continues to increase as DR increases, until the profiles reach the MDR asymptote as shown in figure 8(b–e). The DR in $C_i = 1000$ and 2000 w.p.p.m. flows, the velocity profiles of which are shown in figure 8(d, e), are all at MDR or near MDR. It is clearly shown that increasing the injection concentration from 1000 to 2000 w.p.p.m. does not increase the DR over the MDR limit. In this sense, the extra polymer injected is 'wasted'. However, the $C_i = 2000$ w.p.p.m. flow does maintain a longer streamwise MDR distance than the $C_i = 1000$, which is obvious when we compare DR at position $x4$.

The few data points under $y^+ < 10$ are lower than the $u^+ = y^+$ line for $C_i = 1000$ and 2000 w.p.p.m. flows as shown in figure 8(*d, e*). The reason is that the viscosity of water is used in the normalization of velocity, including the positions close to the wall, where the viscosity is actually higher owing to the presence of polymer. It is clear that the higher the injected polymer concentration, the greater the deviation from the $u^+ = y^+$ lines owing to the viscosity effect. Unfortunately, it is difficult, if not impossible, to determine the correct near-wall viscosity. An attempt has been made to estimate roughly the near-wall polymer solution viscosity as follows. Assuming the mean near-wall velocity measurement is accurate enough (which may not be strictly true owing to the difficulties related to PIV measurement at the near-wall region with high-concentration polymer solution), the near-wall solution viscosity can be estimated by imposing $u^+ = y^+$ (i.e. $u/u_\tau = yu_\tau/\nu$) in the sublayer region. The left-hand axis in figure 9 shows the near-wall viscosity for $C_i = 1000$ and 2000 w.p.p.m. flows, while the right-hand axis shows u^+ *vs.* y^+ as normalized by that viscosity. The viscosity is seen to reduce smoothly from the wall towards the outer layer and merges to the water viscosity outside the sublayer. The viscosity close to the wall can be up to 10 times that of the water viscosity. If the relationship between polymer solution viscosity and polymer concentration is known accurately, this method can, potentially, be used to estimate the local polymer concentrations at high injection concentrations. Certainly, this method can only be an additional tool for concentration measurements but not a complete one. It can only measure high polymer concentrations within the sublayer and the PIV system should be optimized for sublayer measurement.

4.2. *Velocity fluctuation profiles*

The u_{rms} profiles in $C_i = 500$ w.p.p.m. flow are plotted in different coordinates and are shown in figure 10, where $u^+_{rms} = u_{rms}/u_\tau$. The u_{rms} profiles for the other C_i values show a similar trend and are not shown for brevity. Fontaine, Petrie & Brungart (1992) plotted most of their u_{rms} profiles in polymer flow by using the Newtonian flow shear velocity (not the shear velocity in polymer flow, which should more properly be used). They concluded that 'Streamwise r.m.s. velocity fluctuations are suppressed near the wall owing to the high polymer concentration layer there and increase farther out in the boundary layer. The u' profile peaks at roughly the edge of the polymer layer on the wall.' The current results in figure 10 agree with those statements but provide a clearer interpretation. The un-normalized peak values for polymer flow are smaller than those of the corresponding Newtonian flows. However, the u_{rms} value is physically increased for $y/\delta \sim 0.1$ to 0.5. This is different from the Reynolds shear stress (discussed later) in that the un-normalized Reynolds shear stress is never higher than that of the Newtonian flow. The u_{rms} peak value locations are also shifted outward to higher y/δ value. For the $C_i = 500$ w.p.p.m. case shown, the locations are $y/\delta \sim 0.1$ and $y^+ \sim 80$. Although the peak values for Newtonian flow are not resolved in the current study, they are about $u^+_{rms} \sim 2.6$ at $y^+ \sim 10$ to 20 for lower Reynolds number flows (Fernholz & Finley 1996). With this, it can be seen that the u^+_{rms} peak values in polymer flow are much higher than those of Newtonian flows and this finding agrees with the study of homogeneous polymer channel flow by Warholic *et al.* (1999). In fact, the value of u_{rms} in wall units is higher than that of the Newtonian flow throughout the entire boundary layer.

Figure 10 (*d–e*) shows the improved normalization (DeGraaff & Eaton 2000) of u_{rms} with mixed inner and outer velocity scaling, i.e. $u^2_{rms}/(u_\tau U)$. The classically normalized u_{rms} profiles at positions $x06$ and $x1$ in polymer flow deviate from the profiles at other locations, as shown in figure 10(*b, c*), while the u_{rms} profiles with the improved

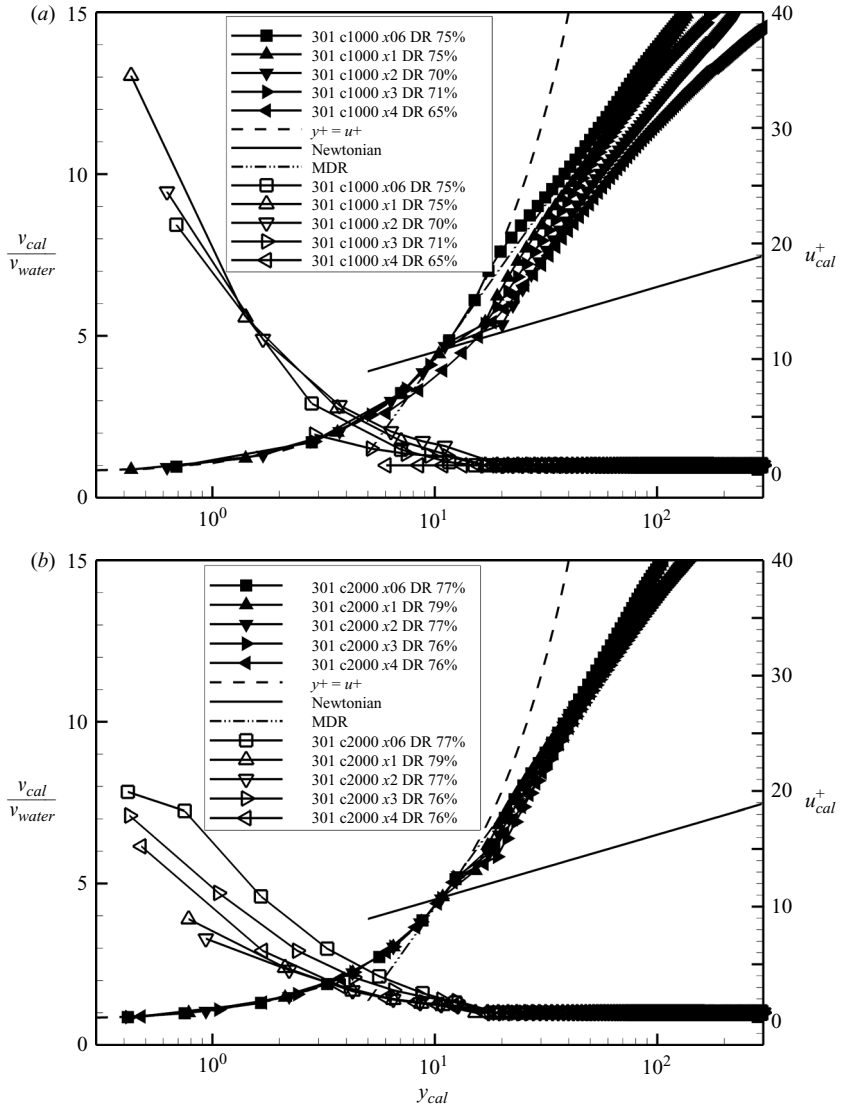

FIGURE 9. Viscosity of the polymer solution in the near-wall region.

normalization at position $x06$ and $x1$, shown in figure 10(*d, e*), have much less deviation from the profiles at other locations. Furthermore, by comparing figure 10*d* with figure 10*b*, the improved normalization also show less deviation of profiles in polymer flows from those in Newtonian flows for the whole BL. This confirms that the improved normalization not only collapses the Newtonian and polymer profiles individually, it also collapses the Newtonian profiles with the polymer profiles.

The v_{rms} profiles for $C_i = 500$ w.p.p.m. are shown in figure 11, $v^+_{rms} = v_{rms}/u_\tau$. The v_{rms} profiles for the other C_i values show a similar trend and are not shown for brevity. The v_{rms} values in polymer flow are roughly constant throughout the whole boundary layer while the corresponding values in Newtonian flow increase towards the wall, reach a peak value, and then reduce quickly close to the wall. The value of v_{rms} should reduce to zero at the wall in both Newtonian flow and polymer flow,

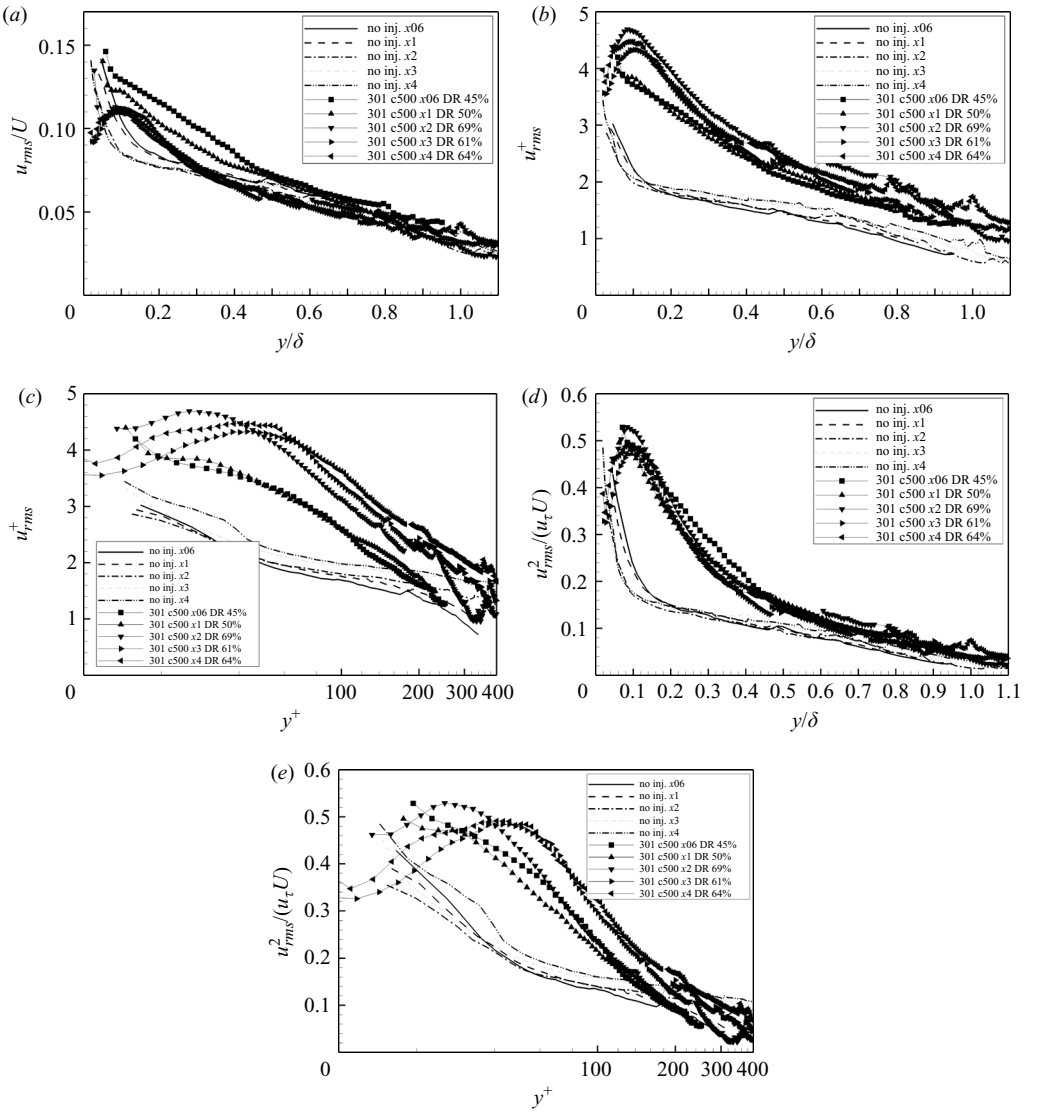

FIGURE 10. u_{rms} profiles in polymer drag-reduced flow.

but the PIV measurement could not resolve it. The v_{rms} in polymer flow is smaller when un-normalized and is larger in wall units than that of the Newtonian flow, as a consequence of the normalization. Smaller un-normalized v_{rms} agrees with results in boundary-layer flow by Fontaine *et al.* (1992) and homogeneous polymer channel flow by Warholic *et al.* (1999). However, the normalized profiles, v^+_{rms}, are different in the current study. Most v^+_{rms} profiles in polymer flows by Fontaine *et al.* (1992) were normalized by the Newtonian flow shear velocity and not the polymer flow shear velocity. They did provide two v^+_{rms} profiles normalized by estimated shear velocity in polymer flows and showed that the v^+_{rms} values are lower in polymer flow than those in Newtonian flow with small differences. The v^+_{rms} values in a homogeneous polymer channel by Warholic *et al.* (1999) were also lower in polymer flows than those in Newtonian flows. It is not clear why the current study shows different trends of v^+_{rms}

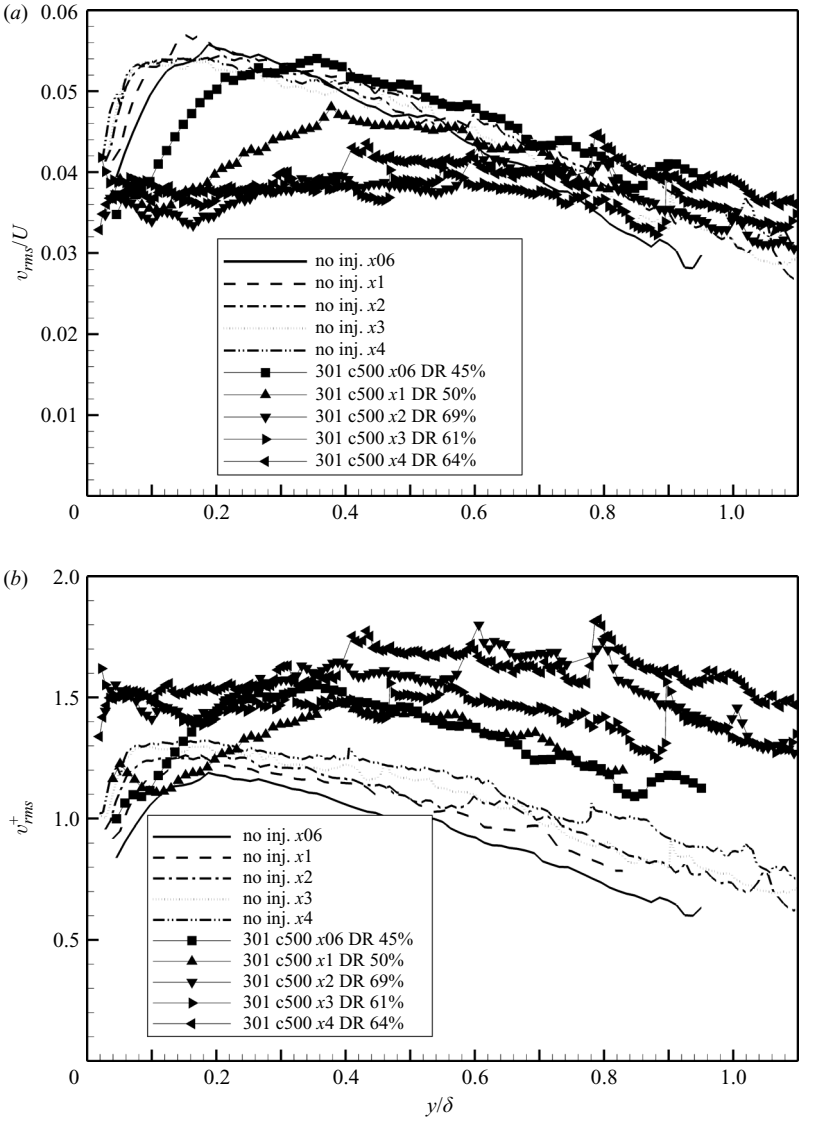

FIGURE 11. v_{rms} profiles in polymer drag-reduced flow.

values with those by Fontaine *et al.* (1992) in boundary-layer flow and Warholic *et al.* (1999) in homogeneous polymer channel.

4.3. *Reynolds stress profiles*

The Reynolds shear stress profiles normalized by the outer flow parameters are shown in figure 12. The general features shown are that the Reynolds shear stress in polymer flow is being reduced and the reduction is larger when the DR is higher and it is in agreement with Fontaine *et al.* (1992) and Warholic *et al.* (1999). In most of the cases in the current study, the Reynolds shear stress in the polymer flows are only reduced at smaller y/δ while being unaffected at larger y/δ. When the polymer flow with low injection concentration is compared to the Newtonian flow, i.e. $C_i = 100$ w.p.p.m. shown in figure 12(a), the Reynolds shear stress in the polymer flow is smaller for

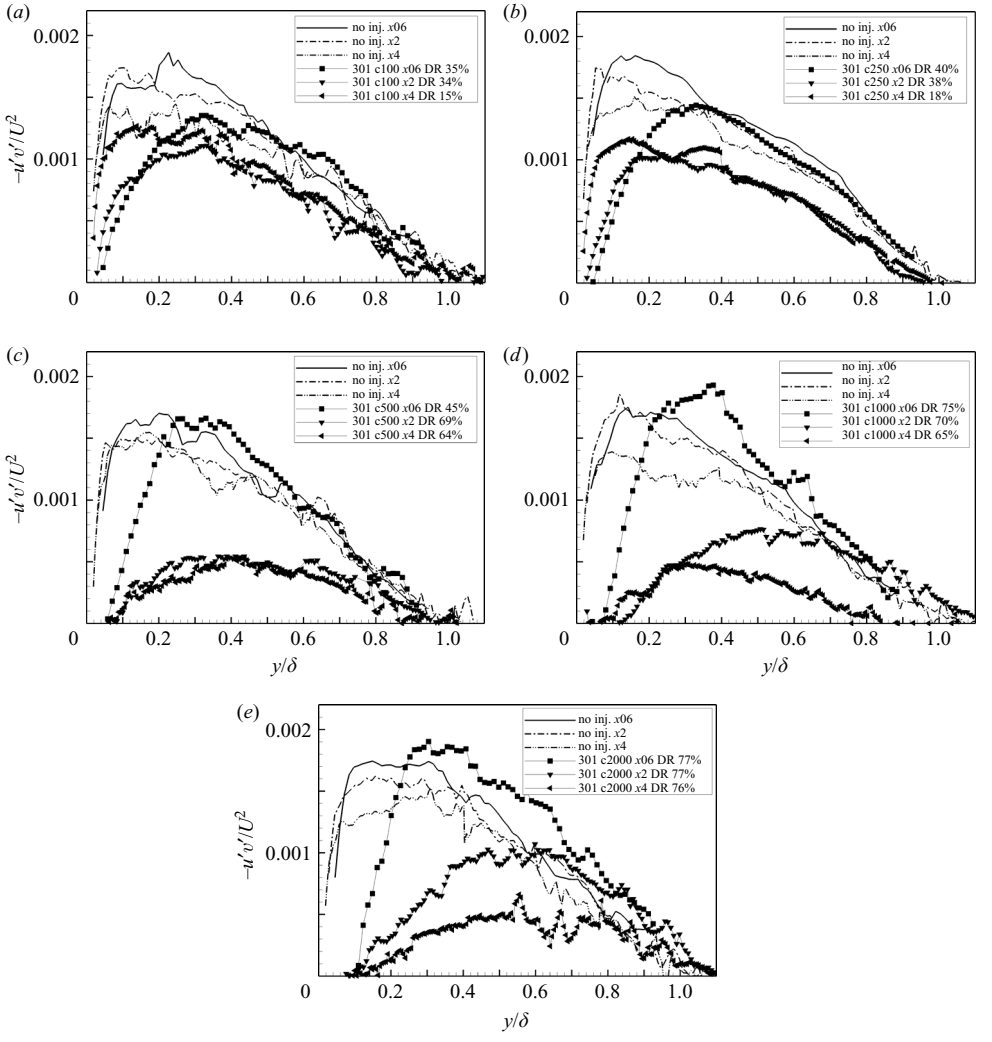

FIGURE 12. Reynolds shear stress in outer coordinates.

$y/\delta < 0.5$, but similar for $y/\delta > 0.5$. The Reynolds shear stress at position $x2$ for $C_i = 1000$ w.p.p.m. is reduced at $y/\delta < 0.6$ and is similar to that of the Newtonian flow at larger y/δ. The reduction of Reynolds shear stress can spread to the entire boundary layer, e.g. at position $x4$ for $C_i = 1000$ w.p.p.m. as shown in figure 12(d).

It is worth paying attention to position $x06$ for the cases of higher injection concentrations, $C_i = 500$, 1000 and 2000 w.p.p.m., shown in figures 12(c), 12(d) and 12(e), respectively. The Reynolds shear stress at position $x06$ is not affected for $y/\delta > 0.2$, while in the inner region, it is sharply reduced to zero. This shows that the effect of polymer on Reynolds shear stress spreads away from the wall to the outer parts of the boundary layer gradually. This feature generally agrees with how the injected polymer diffuses away from the wall with increasing downstream distance. However, the relation between the polymer diffusion and the reduction of Reynolds shear stress is complex and should not be considered a one-to-one relationship. When comparing Reynolds shear stress in polymer flows at $y/\delta = 0.3$ and streamwise

location $x06$ with $C_i = 100$ and 500 w.p.p.m., as shown in figures 12(a) and 12(c), it is seen that the Reynolds shear stress is reduced for the $C_i = 100$ w.p.p.m. flow, but not the $C_i = 500$ w.p.p.m. flow. The reason is that the 500 w.p.p.m. injection more effectively reduces the skin friction and the near-wall turbulent activity than does the 100 w.p.p.m. injection. The polymer in $C_i = 500$ w.p.p.m. flow is transported away from the wall at a slower rate than that of the $C_i = 100$ w.p.p.m. flow owing to the reduced turbulent activity so that the polymer has not reached $y/\delta = 0.3$ at streamwise position $x06$ for the $C_i = 500$ w.p.p.m. flow. This is consistent with PLIF results (Fontaine *et al.* 1992 and its references; Somandepalli 2006) that polymer is transported away from the wall at a much slower rate than a passive scalar. Considering position $x06$ in $C_i = 500$ w.p.p.m. flow, from the similarity of the Reynolds shear stress peak values of both Newtonian flow and polymer flow, we might conclude that there is no DR. However, the mean velocity profiles are already showing high DR and even MDR (figure 7). One explanation of this is that the mean velocity responds quickly to the flow condition change, i.e. suddenly reduced wall shear stress. However, it takes a much longer time for the entire Reynolds shear stress profile to adjust to the same change, i.e. only the inner part ($y/\delta < 0.2$) has been affected, but the outer part ($y/\delta > 0.2$) has not yet been affected. This seems to confirm an independence between near-wall turbulent structures (which are directly affected by polymers) and turbulence in the log layer, as proposed by Jimenez & Pinelli (1999). The Reynolds shear stress in flows with injection concentrations greater than 500 w.p.p.m. is almost zero for $y/\delta \sim 0$ to 0.1 and signifies high DR.

The Reynolds shear stress normalized by wall units ($-u'v'^{+} = -u'v'/u_\tau^2$) is plotted against y/δ (figure 13). The common feature for all the profiles is that the position of the peak value in the polymer flow shifts outward, i.e. to greater y/δ value. The shift is larger when the DR is higher. The peak locations for position $x2$ and $x4$ at $C_i = 1000$ and 2000 w.p.p.m. are at $y/\delta \sim 0.6$. While the peak values are about the same for both Newtonian flow and polymer flow at $C_i = 100$ w.p.p.m., the peak value for $C_i = 250$ and 500 w.p.p.m. flow at position $x06$ is much higher than that of the Newtonian flow. This is expected since the un-normalized Reynolds shear stress peak value is about the same as that of the Newtonian flow, but the wall shear stress has been reduced. The peak values at position $x2$ for $C_i = 1000$ w.p.p.m. and at positions $x2$ and $x4$ for $C_i = 2000$ w.p.p.m. are also much higher than those of the Newtonian flows. It should be noted that the higher Reynolds shear stress in plus units is not because it is being increased, but rather because the Reynolds shear stress is not reducing quickly enough and the flow is not in an equilibrium state. It may appear strange that DR flow can have high Reynolds stress in wall units, but it is reasonable when compared with the weak relaminarization of a boundary layer by strong convective acceleration. As described in White (1991): 'the turbulence does not disappear, but mean parameters such as the velocity profile and skin friction approach laminar values. Turbulence becomes smaller only in an absolute sense: ($-\overline{u'v'}$) remains almost constant during the laminarization process but is a sharply decreasing fraction of the stream energy U_e^2.' That feature is very similar to those observed in the current study since, in the weak relaminarization of the boundary layer, the 'almost constant' Reynolds stress increases in wall units since the skin friction has been reduced. This unique feature can be used to roughly judge whether the flow is in equilibrium: if the Reynolds shear stress in polymer flow is the same as that of Newtonian flow in wall units, it indicates that the flow is in an equilibrium state; if it is much higher than unity (typically away from the wall), it tells us that that part of the boundary layer has not adjusted to the changed wall shear stress, and hence the flow is not in equilibrium.

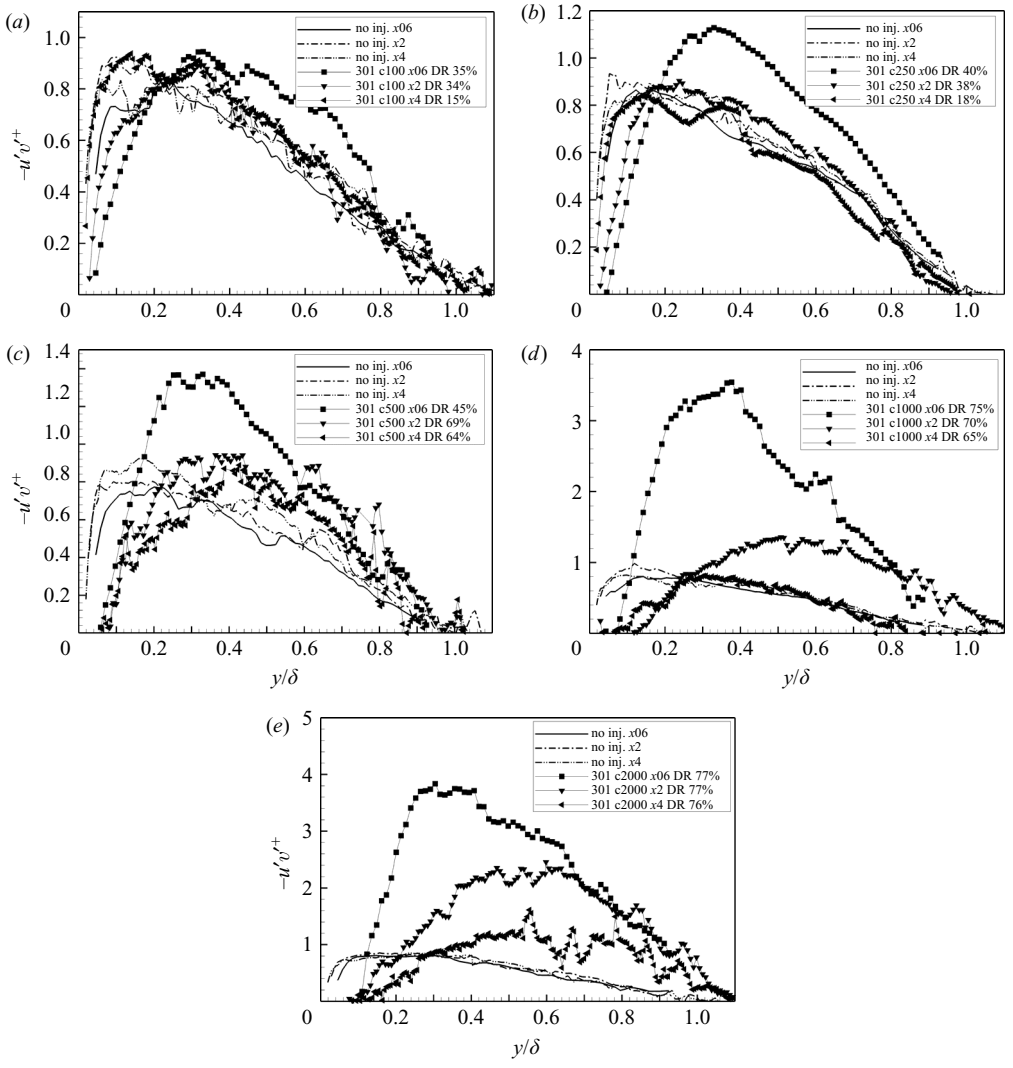

FIGURE 13. Reynolds shear stress in wall units.

4.4. *Higher-order turbulence statistics*

Figure 14 shows the turbulent energy production $[(-\overline{u'v'})(\mathrm{d}u/\mathrm{d}y)]^+$ $(=(-\overline{u'v'})(\mathrm{d}u/\mathrm{d}y)(\nu/u_\tau^4))$ profiles measured for the different cases of drag reduction. For the water-injection case, shown by the lines with no symbols, there is very little or no change seen in the magnitude and distribution of the turbulent energy production in the near-wall region along the length of the plate. The 100 w.p.p.m. injection case, shown in figure 14(*a*), shows a slight decrease in the magnitude of production at position $x06$. Further downstream, this magnitude increases to values similar to those in the water-injection case. When the injection concentration is increased to 250 w.p.p.m. (figure 14*b*), the peaks in the production profiles at positions $x06$ and $x2$ occur further away from the wall, at $y^+ = 20$, where their magnitudes are also lower than those observed in the water-injection case. At these locations, the drag reductions measured are relatively high. At this injection concentration, further downstream, at position $x4$

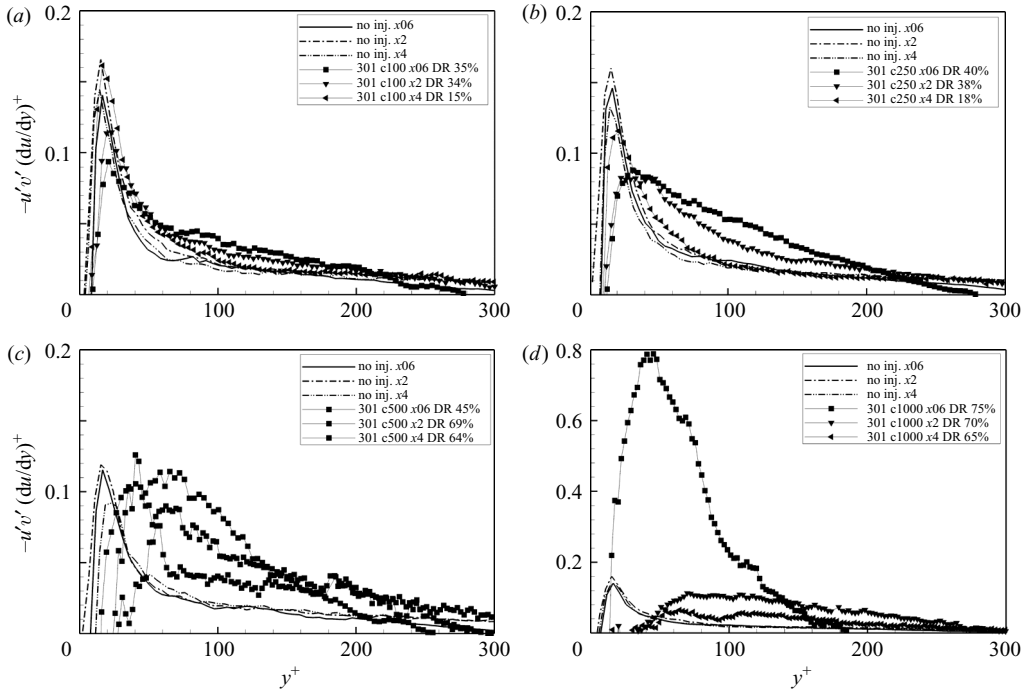

FIGURE 14. Production profiles in polymer drag-reduced flow.

where the drag reduction decreases, the turbulent energy production profile regains its water-like behaviour with a peak located very close to the wall and a magnitude greater than that of other upstream locations. For the case of higher concentrations of 500 w.p.p.m. and 1000 w.p.p.m., shown in figures 14(*c*) and 14(*d*), the peaks in the production profiles shift further outward from the wall with increasing concentration. Close to the wall, the production of turbulent kinetic energy is suppressed by the action of the polymer.

Figure 15 shows the momentum eddy diffusivity $[(-\overline{u'v'})/(\mathrm{d}u/\mathrm{d}y)]^+$ $(= (1/\nu)(-\overline{u'v'})/(\mathrm{d}u/\mathrm{d}y))$ as estimated from the PIV data for various concentrations of the injected polymer. For the 250 w.p.p.m. polymer injection case, shown in figure 15(*a*), at positions $x06$ and $x2$, the momentum eddy diffusivity is suppressed across the boundary layer relative to the water-injection case. As the flow develops and the drag reduction reduces, at position $x4$, the profile of the eddy diffusivity also becomes similar to that of water. For the higher concentration cases (500 w.p.p.m. shown in figure 15*b* and 1000 w.p.p.m. shown in figure 15*c*), the suppression of the eddy diffusivity increases along the length of the flat plate with the greatest amount of suppression relative to water injection seen at position $x4$. The location of the peak and the slope of the profile close to the wall also change progressively with increasing downstream distance in these cases. The trends observed here for the momentum eddy diffusivity are similar to those observed by Gupta, Sureshkumar & Khomami (2005) in their simulations of scalar transport in a polymer drag-reduced turbulent channel flow.

In polymer flows, the production and the momentum eddy diffusion are either equivalent to or smaller than those of the corresponding Newtonian flows. The difference is larger with higher DR. The only exception is the production at

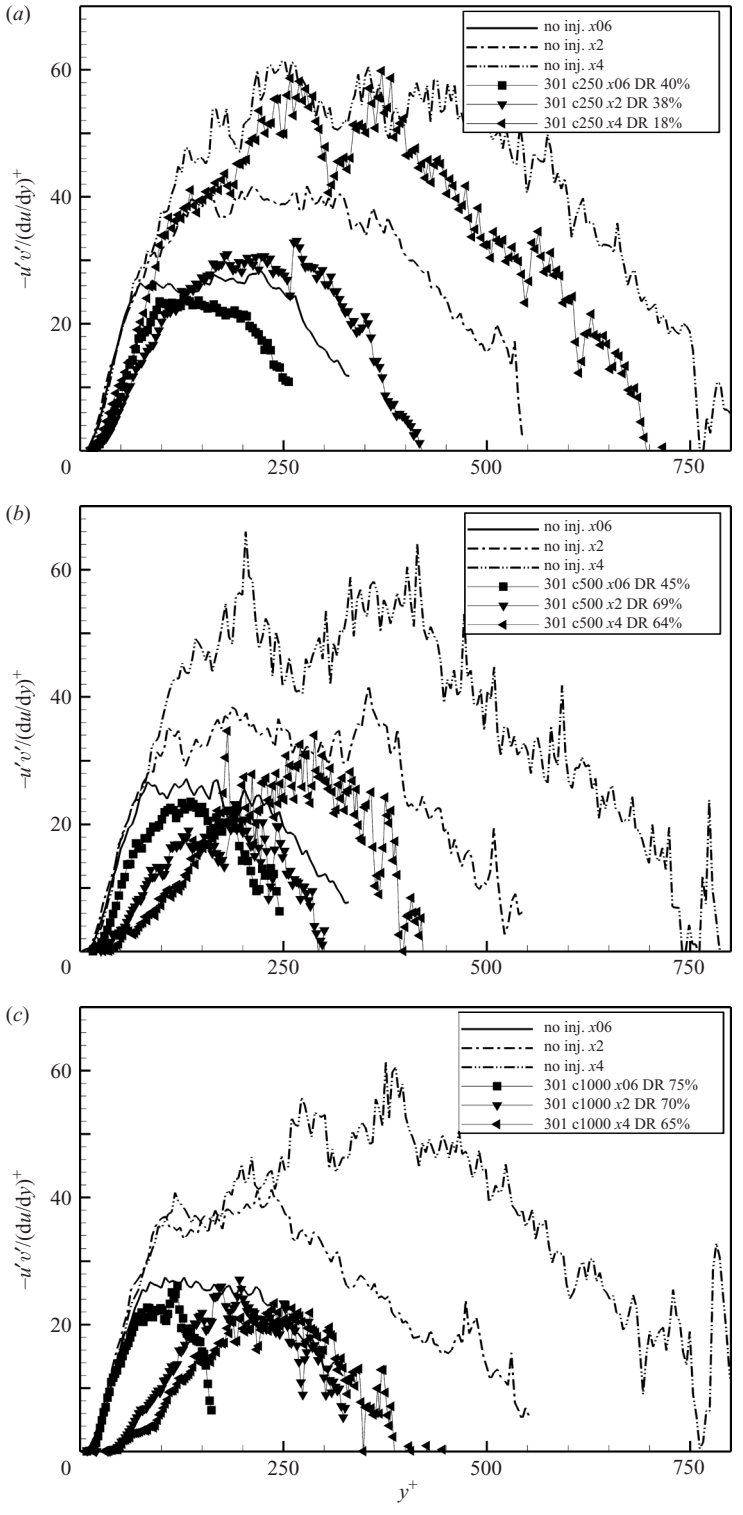

FIGURE 15. Momentum eddy diffusion in polymer drag-reduced flow.

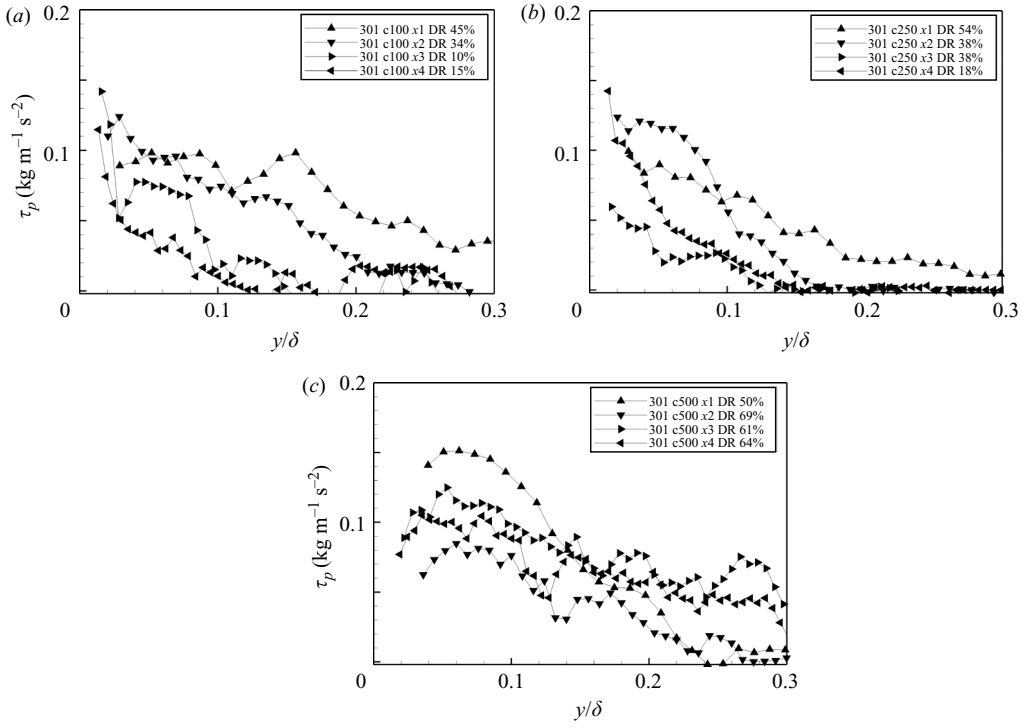

FIGURE 16. Streamwise development of polymer stress.

position $x06$ with $C_i = 1000$ w.p.p.m. and it is due to the non-equilibrium flow condition discussed above. The smaller production and momentum eddy diffusivity are consistent with the fact that the skin friction is reduced, turbulent activity is reduced, and the flow is evolving from turbulent flow towards laminar flow. It also supports the fact that the injected polymer moves away from the wall at a much smaller rate than that of a passive dye (Fontaine *et al.* 1992 and its references, Somandepalli 2006).

5. Polymer stress profiles

Streamwise development of polymer stress profiles for $C_i = 100$, 250 and 500 w.p.p.m. are shown in figure 16. The polymer stress shown is not normalized and has units of kg $m^{-1} s^{-2}$, which is the same as the total shear stress in figure 4. The polymer stress is found to be significant for $y/\delta < 0.3$ and negligible in the outer part of the boundary layer. The polymer stress is proportional to DR for the $C_i = 100$ w.p.p.m. flow, but not for the $C_i = 250$ and 500 w.p.p.m. flows. It may appear surprising that the magnitude of the polymer stress is not proportional to DR, i.e. high DR can correspond to low polymer stress. However, the interaction between injected polymers and the turbulence in a developing boundary-layer flow is complex and it produces an equally complex relationship between polymer stress and DR (Dimitropoulos *et al.* 2005), unlike the case of fully developed turbulent channel flows. By considering that the $C_i = 100$ w.p.p.m. flow is entirely in the depletion region, it is seen that polymer stress is proportional to the DR value in this case. Figure 17 shows the polymer stress at fixed streamwise positions for both COA and

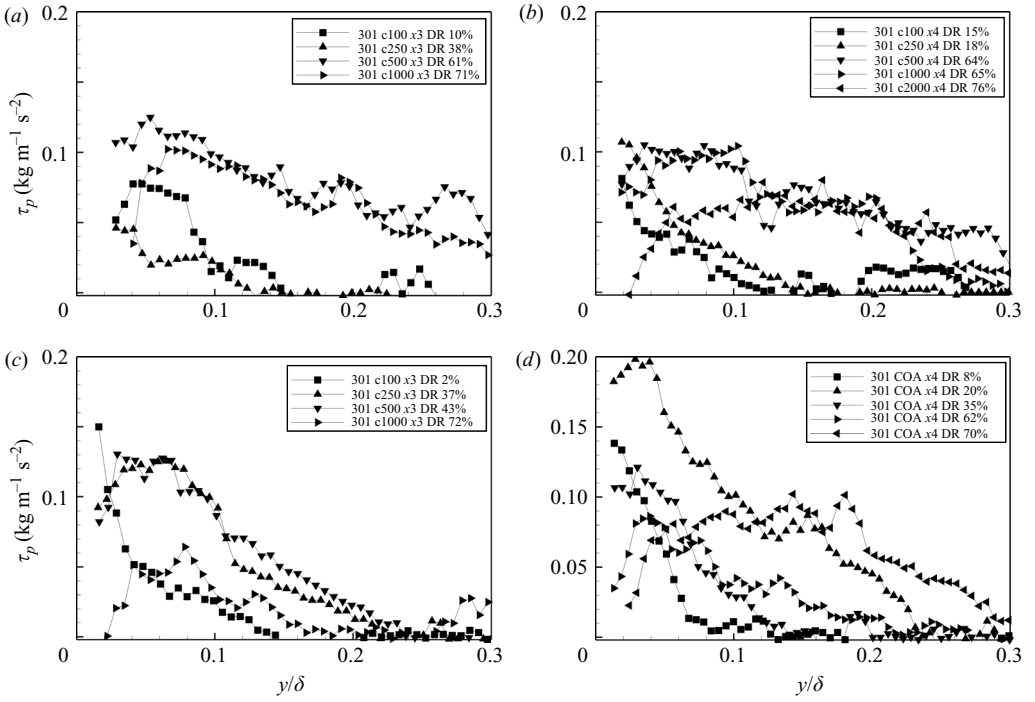

FIGURE 17. Polymer stress profiles at fixed streamwise location for different injection concentrations.

301 with different injection concentrations. For higher concentrations, it is clear that polymer stress is not proportional to the DR value since the flows at that location are in different DR regions owing to the different injection concentrations. This is true for both COA and 301 except that the estimated polymer stress values for COA are slightly higher than that of 301.

The reason that polymer stress is not always proportional to DR can be rationalized by the following hypothetical mechanism of the polymer and turbulent activity interaction cycle: when the polymer is first injected into the TBL, it quickly becomes effective in reducing turbulent activity, leading to increased polymer stress and increasing DR in the development region; further downstream, in the steady-state region (sometime the regions of high DR or MDR), the reduced turbulent intensity allows the polymer to be less stretched and still maintain high DR so that the polymer stress is not necessarily high. The relatively low polymer stress at high DR is also due to the fact that the skin friction (hence the total shear stress) being already reduced is such that the magnitude of the polymer stress must be small. However, the polymer stress can have a high contribution to the total shear stress, as will be shown in the stress balance section below. Even further downstream, in the depletion region, as the turbulent activity regains strength, the DR begins to decrease while the remaining polymer near the wall becomes active and thus generates polymer stress. In this hypothetical cycle, the polymer stress and the drag reduction of the flow are not always synchronized since the turbulent state of the flow and polymer, and their integrated history, are important; there is a phase lag associated with the polymer activity as it responds to the turbulence and this phase difference allows the possibility

Newtonian flow					
Position	I%	II%	III%	IV%	Err%
$x1$	8.8	65.4	23.7	0	−2.1
$x2$	6.9	67.5	23.6	0	−2.0
$x3$	5.8	72.3	19.4	0	−2.5
$x4$	5.1	67.6	24.1	0	−3.2

TABLE 5. Dynamical contributions to the skin-friction in Newtonian ZPG TBL.

PEO WSR-301; concentration = 100 w.p.p.m.; $Q_i/Q_s = 0.78$						
Position	DR	I%	II%	III%	IV%	Err%
$x1$	45	16.6	62.6	8.5	16.7	4.5
$x2$	34	10.7	60.7	22.1	9.3	2.8
$x3$	10	6.5	64.9	24.1	5.1	0.6
$x4$	15	6.6	68.4	21.1	5.8	1.9

TABLE 6. Dynamical contributions to the skin-friction in polymer flow with injection concentration of 100 w.p.p.m.

of high DR with low polymer stress. Hence, there is not a one-to-one relationship between polymer stress and DR, except in the depletion region.

6. Stress balance in the TBL

With the total shear stress profiles and the polymer stress profiles obtained by using the $(1 - y/\delta)$ fitting, the dynamical contributions to the skin-friction in ZPG TBL flows (equation (2) and White *et al.* 2006) are evaluated by integrating each term directly, with results shown in table 5 for Newtonian flow and tables 6–9 for polymer flows. Since equation (1) is valid for a dilute polymer 'ocean' and not valid in a highly nonlinear viscoelastic solution, we apply the analysis only at the locations where sufficient dilution of the polymer has occurred. A total of 25 different cases for the polymer WSR-301 are possible (5 concentrations × 5 measuring stations). However, we believe that for all the 5 streamwise positions in the 2000 w.p.p.m. injection case and at the first 3 positions – $x06$, $x1$ and $x2$ – in the 1000 w.p.p.m. injection case, the polymer is not sufficiently dilute. Eliminating these 8 cases leaves a maximum of 17 cases which can be properly analysed. To be conservative, the analysis was performed for the 14 cases shown in tables 6–9 where equation (1) is believed to be valid. The tables give the percentage contributions of each term to the skin friction, and the error in the predicted skin friction obtained from summing the four terms when compared to the measured value. The role of the polymer stress in the overall DR can thus be ascertained.

The Newtonian flow in table 5 shows that the contributions of the viscous term (term I), Reynolds stress (term II) and total stress gradient (term III) to the skin friction are 5∼9%, 65∼70% and 20∼23%, respectively. The polymer flow at position $x1$ (DR% = 45%) in table 6 shows that the contribution of term I increases significantly to 16.6%. However, the absolute values (not shown) of term I are the same for both polymer flow and the corresponding Newtonian flow. The percentage increase of its contribution is only a result of the reduced skin friction. The contributions of

PEO WSR-301; concentration = 250 w.p.p.m.; $Q_i/Q_s = 0.82$

Position	DR	I%	II%	III%	IV%	Err%
$x1$	54	19.0	68.7	0.6	14.9	3.2
$x2$	38	11.1	60.0	20.0	11.2	2.2
$x3$	38	9.4	71.0	15.6	5.5	1.5
$x4$	18	6.2	61.6	28.2	5.9	1.9

TABLE 7. Dynamical contributions to the skin-friction in polymer flow with injection concentration of 250 w.p.p.m.

PEO WSR-301; concentration = 500 w.p.p.m.; $Q_i/Q_s = 0.79$

Position	DR	I%	II%	III%	IV%	Err%
$x1$	50	17.1	64.5	1.8	19.3	2.8
$x2$	69	21.5	52.7	7.4	17.6	−0.8
$x3$	61	14.6	41.6	16.5	27.0	−0.3
$x4$	64	14.0	45.4	16.5	24.5	0.3

TABLE 8. Dynamical contributions to the skin-friction in polymer flow with injection concentration of 500 w.p.p.m.

PEO WSR-301; concentration = 1000 w.p.p.m.; $Q_i/Q_s = 0.77$

Position	DR	I%	II%	III%	IV%	Err%
$x3$	71	20.4	49.6	6.7	25.1	1.8
$x4$	65	14.7	42.1	23.3	20.5	0.6

TABLE 9. Dynamical contributions to the skin-friction in polymer flow with injection concentration of 1000 w.p.p.m.

terms II and III are both reduced in polymer flow and the reductions are different at different conditions. The general trend shown in tables 6–9 is as follows: at upstream locations, term II is only slightly reduced while term III is significantly reduced; further downstream, the reduction of term II becomes more significant while the reduction of term III becomes less significant. This trend is best seen in the near MDR flow in table 9 from position $x3$ (DR% = 71%) to $x4$ (DR% = 65%) – term II is reduced from 49.6% to 42.1%; while term III increases from 6.7% to 23.3%. For all the cases shown in tables 6–9, the highest contribution of polymer stress (term IV) to the skin friction is about 25%, which shows that polymer stress can be an important contributor to the skin friction. The contribution of polymer stress is roughly proportional to the DR values for the cases shown in tables 6–7, i.e. higher contribution of term IV in higher DR flow. This appears to be because the flow in these two cases is in the DR depletion region. The contribution of polymer stress is not proportional to DR when the flow goes through different DR regions as shown in table 8, where the DR% increases from 50% ($x1$) to 69% ($x2$) (development region), then reduces slightly and finally remains constant from positions $x3$ to $x4$ (steady-state region). The trend of the polymer stress contribution to the skin friction shown in table 8 is consistent with the above proposed polymer and turbulent activity interaction cycle. The contribution of term IV is higher at $x1$ (DR% = 50%) than

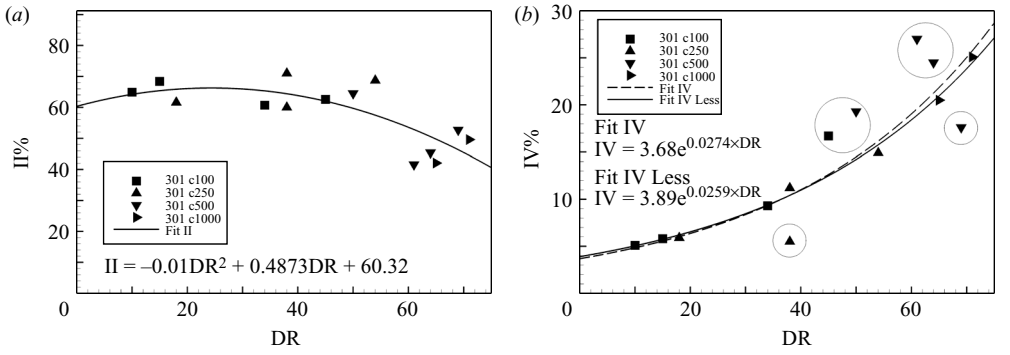

FIGURE 18. The contributions to the skin friction: (*a*) the Reynolds stress (term II); (*b*) the polymer stress (term IV), where 'Fit IV' uses all the data and 'Fit IV Less' does not use the data in the circles.

that at $x2$ (DR% = 69%) because the flow is in the development region. In this region, the polymer is more active due to the strong turbulent activity in the incoming flow so that polymer stress has a larger contribution. While at position $x2$ (DR% = 69%), the turbulent activity has been significantly reduced and the polymer is less active so that it has a relatively smaller contribution. Further downstream, the DR decreases slightly which indicates that the turbulent activity becomes relatively stronger. As a result, the polymers become more active again and hence polymer stress (term IV) has a larger contribution.

The contributions of the Reynolds stress (term II) and the polymer stress (term IV) to the skin friction are plotted versus DR in figure 18. The contribution of the Reynolds stress shown in figure 18 (*a*) is relatively constant for DR less than 40 and reduces at higher DR. However, even at high DR, the contribution of Reynolds stress is still significant above 40%. There are two curve fits of the polymer stress contribution in figure 18 (*b*). The first fit is done by using all the data points and is shown as the dashed line. The second fit, 'Fit IV Less', is done with the six data points in the circles removed. Those six data points are not entirely in the depletion region so that the polymer stress contribution may not be proportional to DR. By removing those six data points, the polymer stress contributions lie neatly on the simple exponential curve fit and is thus considered being proportional to DR. This suggests that the polymer stress contribution is not always proportional to DR, but is proportional to DR in the depletion region.

7. Dynamical stress balance in channel flow

We compare the polymer stress in the TBL with inhomogeneous injection to those found in channel flows with homogeneous polymer distribution. Such data have been provided by Warholic *et al.* (1999). To perform the analysis, we note that the corresponding equation for the dynamical contributions in the channel flow is given by White *et al.* (2006) as

$$C_f \equiv \tau_w/\left(\tfrac{1}{2}\rho U_m^2\right) = \underbrace{\frac{6}{Re_h}}_{\mathrm{I}} + \underbrace{6\int_0^1 (1-y^{**})(-\overline{u'v'}^{*})\mathrm{d}y^{**}}_{\mathrm{II}} + \underbrace{6\int_0^1 (1-y^{**})\bar{\tau}_p \mathrm{d}y^{**}}_{\mathrm{III}}, \qquad (4)$$

	I%	II%	III%	Err%
Water	8.8	91.2	0	N/A
DR = 38	15.0	60.4	23.2	−1.3
DR = 55	20.0	19.4	61.3	0.7
DR = 64	23.3	1.1	63.2	−12.4
DR = 69	28.4	9.9	57.9	−3.7

TABLE 10. Dynamical contributions to the skin-friction in homogeneous channel flow derived from data of Warholic *et al.* (1999).

where Re_h is the Reynolds number based on channel mean velocity U_m and channel half-height h, y^{**} is the wall normal coordinate normalized by h, $-\overline{u'v'}^{*}$ is the Reynolds shear stress normalized by U_m^2 and $\bar{\tau}_p$ is the polymer stress normalized by ρU_m^2 for a polymer solution. Using the data from figures 13 and 14 of Warholic *et al.* (1999) produces the results shown in table 10. The agreement between DR and prediction given by the sum of the three terms is satisfactory for water and most DR cases, with errors of less than 4%. The exception is the DR = 64% case. Here, the error comes from term II since the measured Reynolds stress in the original paper was very small so there is a large digitization error.

An important comparison of the homogeneous channel at MDR to the inhomogeneous TBL at MDR is that the former shows a polymer stress contribution of ~60% while the latter shows ~25%. This appears to be a fundamental difference associated with inhomogeneous and homogeneous distribution of polymer at MDR. In the inhomogeneous case, the Reynolds stress is decreased significantly close to the wall, but less so further from the wall at MDR. The $(1 - y/\delta)$ fitting and equations (2) and (4) suggest that contributions to the skin friction from the Reynolds stress away from the wall will play a lesser role in the overall DR. In the homogeneous channel case, while the Reynolds stresses are reduced across the entire channel width, the $(1 - y/\delta)$ weighting still shows that it is primarily the reductions close to the wall that produce the dominant DR effect.

8. Sketch of three DR regions

The sketch of the three DR regions, i.e. development, steady-state and depletion, and some associated features are shown in figure 19 (*a*). This figure is intended to help in summarizing the characteristics of the flow in different conditions. Further experiments and additional data are required in order to obtain a more complete and accurate figure which is beyond the scope of this paper. This figure is an idealized one in that it assumes there exists a 'universal curve' in DR *vs.* $\log_{10}(K)$ space for a given type of polymer and injector arrangement. It should be pointed out that the measured data show a certain degree of scatter as in all real flows, as seen in figure 6. Nevertheless, with the assumption that a single curve exists for a given polymer, figure 19 (*a*) summarizes some key features of the flows with different injection concentrations of the polymer for the three DR regions. It is expected that the length of the steady-state drag-reduction region in flows with high injection concentrations (typically HDR/MDR flows) is longer than that of flows with medium or low injection concentrations. At some condition, the steady-state drag-reduction region for low injection concentration can be very small or may not exist. The flow may not be in equilibrium in the development region (part or whole) and/or part

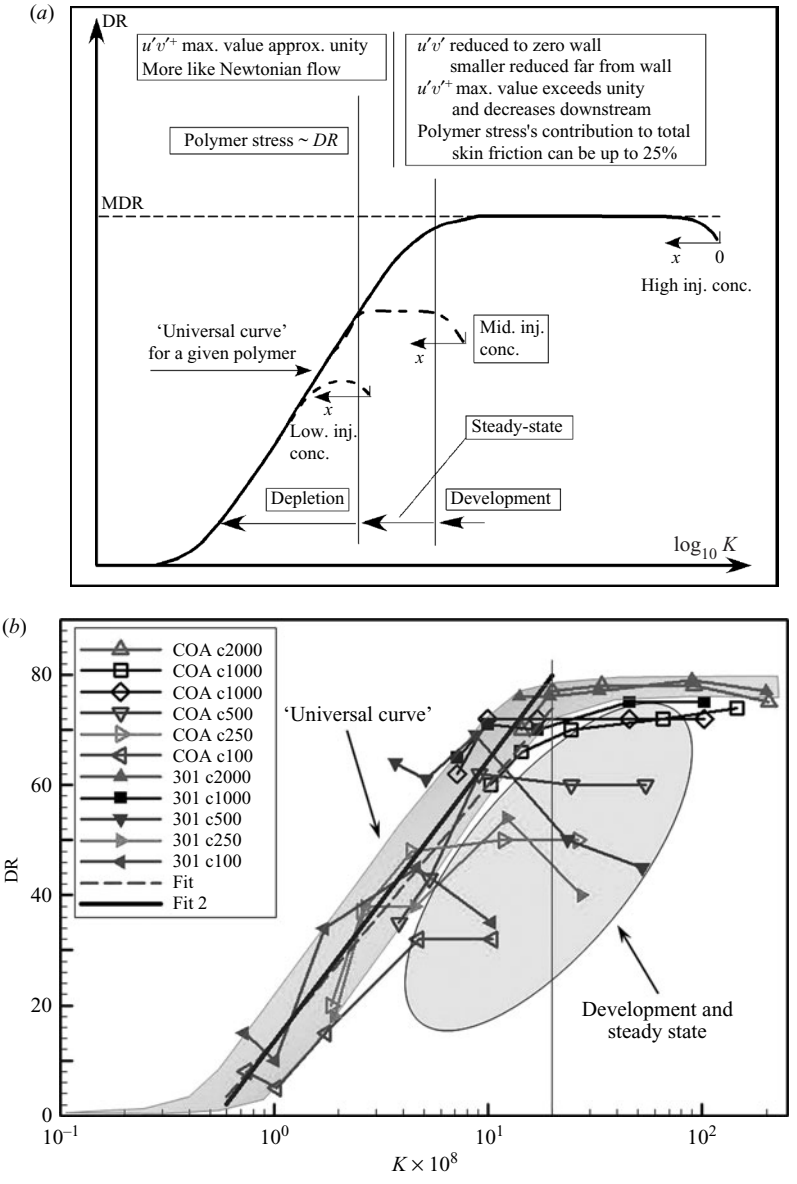

FIGURE 19. Sketch of the drag-reduction evolution of the flow through the three drag-reduction regions. (*a*) the three DR regions are labelled for the medium injection concentration only; (*b*) the dashed line 'Fit', $\mathrm{DR} = 46.3\log_{10}(K \times 10^8) + 13.7$, with all the $K < 20 \times 10^8$ data; the solid black line 'Fit 2', $\mathrm{DR} = 51.1\log_{10}(K \times 10^8) + 13.4$, with the $K < 20 \times 10^8$ data except the four data points in the ellipse.

of the steady-state region. In this region, when the flow is not in equilibrium, the Reynolds shear stress profile observed is different from that of a typical ZPG TBL and shows normalized peak values greater than unity. Further downstream, in the steady-state region (part or whole) and in the depletion region, the flow reaches equilibrium and hence the Reynolds shear stress profile is similar to that seen in a Newtonian ZGP TBL. The polymer stress magnitude is typically proportional to the

observed drag reduction in the depletion region but this is not necessarily true in the other regions. Although the polymer stress magnitudes in the steady-state region may not be very high, the contribution of polymer stress to the skin friction, in this region, can be as high as 25% of the total value.

The experimental data are compared with various fits as shown in figure 19 (*b*). The dashed line fit, $\mathrm{IV} = 3.68\exp(0.0274 \times \mathrm{DR})$, uses all the $K < 20 \times 10^8$ data. The solid black line 'Fit 2', $\mathrm{IV} = 3.89\exp(0.0259 \times \mathrm{DR})$, uses the $K < 20 \times 10^8$ data except the data points in the ellipse. The data in the elliptic curve are in the development and steady-state regions so they should not follow the straight line for the universal decay curve. Although there are only four data points and the difference between the straight line fits with or without the four data points is small, it explicitly emphasizes the distinction between the depletion region and the development and steady-state regions.

9. Conclusions

ZPG TBL DR by polymer injection has been studied for a single injector arrangement. Flows with low DR to MDR have been obtained. A specially developed technique, the $(1-y/\delta)$ fit to the total shear stress profile, has been used in evaluating the skin friction and DR. The current results agree well with the plot of DR *vs.* $\log_{10}(K)$ and the plot can be used as a guide to optimize the usage of polymer for single slot injectors, i.e. the minimum amount of polymer to sustain high DR. Detailed flow field statistics reveal many special features that pertain to boundary-layer flow with polymer injection. The mean velocity in polymer flow is reduced near the wall, increases slightly further away from the wall and then merges with that of the Newtonian flow. The mean velocity profiles in wall units vary from the classical Newtonian flow line, first due to a shift in the profile, then due to a change in the slope of the profile towards the MDR line, as a function of DR. The Reynolds shear stress in polymer flow is reduced and the reduction is greater when the DR is higher. Sometimes, the Reynolds shear stress for polymer flow is only reduced at smaller y/δ and not affected further outward. The polymer effect on Reynolds shear stress spreads outward from the wall to the outer part of the boundary layer gradually with downstream distance. It is shown that the mean velocity responds quickly to the flow condition change, i.e. suddenly reduced wall shear stress, however, it takes a much longer time for the whole Reynolds shear stress profile to adjust to the same change. The Reynolds shear stress profiles in wall units can be higher than unity and this unique feature can be used to judge whether the flow is in equilibrium.

The un-normalized u_{rms} peak values in polymer flow are smaller than those of the corresponding Newtonian flow. However, the un-normalized u_{rms} value is increased further away from the wall. The u_{rms} values in wall units can be higher than that of the Newtonian flow for the entire BL. The improved normalization (DeGraaff & Eaton 2000) of u_{rms} with mixed inner and outer velocity scaling collapses the data much better than the classical normalization. The improved normalization not only collapses the Newtonian and polymer profiles individually, it also collapses the Newtonian profiles with the polymer profiles in the whole BL. The un-normalized v_{rms} values in polymer flow are reduced and are roughly constant throughout the boundary layer. The v_{rms} values in wall units, however, are increased by the normalization. The smaller production and momentum eddy diffusion is consistent with the fact that the skin friction is reduced and the turbulent activity is reduced. It also supports the fact

that the injected polymer is transported away from the wall at a much lower rate than that of a passive dye.

Polymer stress is found to be proportional to DR in the drag depletion region. However, polymer stress is not always proportional to DR, i.e. high DR can correspond to low polymer stress. The interaction between injected polymer and turbulent activity in a developing boundary-layer flow is complex and it produces an equally complex relationship between polymer stress and DR owing to the history effect of the polymer–turbulence interaction. The four-component dynamical contributions to the skin-friction in ZPG TBL flow (White *et al.* 2006) was used and found to predict the skin friction to within a few per cent of the measured values. In addition, it provided quantitative insights into the role of the polymer stress in DR flows. The analysis confirms that polymer stress is proportional to DR only in the depletion portion of the BL and that the polymer stress contribution to the skin friction can be significant at MDR accounting for up to 25% of the total. This is in contrast to drag-reduced channel-flow data for homogeneous polymer distribution where the polymer stresses are responsible for up to 60% of the total skin friction at MDR.

This work is sponsored by Defense Advanced Research Projects Agency (DARPA), Advanced Technology Office, Friction Drag Reduction Program, DARPA Order no. K042/31, K042/13, N115/00, issued by DARPA/CMO, Contract no. MDA972-01-C-0041. The content does not necessarily reflect the position or the policy of the US Government, and no official endorsement should be inferred. The authors thank Drs Chris White and Yves Dubief for helpful discussions of drag reduction in turbulent boundary layers.

REFERENCES

Brungart, T. A., Harbison, W. L., Petrie, H. L. & Merkle, C. L. 1991 A fluorescence technique for measurement of slot injected fluid concentration profiles in a turbulent boundary layer. *Exps. Fluids* **11**, 9–16.

DeGraaff, D. B. & Eaton, J. K. 2000 Reynolds-number scaling of the flat-plate turbulent boundary layer. *J. Fluid Mech.* **422**, 319–346.

Dimitropoulos, C., Sureshkumar, R. & Beris, A. 1998 Direct numerical simulation of viscoelastic turbulent channel flow exhibiting drag reduction: effect of variation of rheological parameters. *J. Non-Newtonian Fluid Mech.* **79**, 433–468.

Dimitropoulos, C., Sureshkumar, R., Beris, A. & Handler, R. 2001 Budgets of Reynolds stress, kinetic energy and streamwise enstrophy in viscoelastic turbulent channel flow. *Phys. Fluids* **13**, 1016–1027.

Dimitropoulos, C. D., Dubief, Y., Shaqfeh, E. S. G., Moin, P. & Lele, S. K. 2005 Direct numerical simulation of polymer-induced drag reduction in turbulent boundary layer flow. *Phys. Fluids* **17**, 011705.

Dubief, Y., White, C., Terrapon, V. E., Shaqfeh, E., Moin, P. & Lele, S. 2004 On the coherent drag-reducing and turbulence-enhancing behaviour of polymers in wall flows. *J. Fluid Mech.* **514**, 271–280.

Erm, L. P. 1988 Low Reynolds-number turbulent boundary layers. PhD thesis, University of Melbourne.

Fernholz, H. H. & Finley, P. J. 1996 The incompressible zero-pressure-gradient turbulent boundary layer: an assessment of the data. *Prog. Aerospace Sci.* **32**, 245–311.

Fontaine, A. A., Petrie, H. L. & Brungart, T. A. 1992 Velocity profile statistics in a turbulent boundary layer with slot-injected polymer. *J. Fluid Mech.* **238**, 435–466.

Fruman, D. H, & Tulin, M. P. 1976 Diffusion of a tangential drag reducing polymer injection of a flat plate at high Reynolds numbers. *J. Ship Res.* **20**, 171–180.

Fukagata, K., Iwamoto, K. & Kasagi, N. 2002 Contribution of Reynolds stress distribution to the skin friction in wall-bounded flows. *Phys. Fluids*, **14**(11), L73–76.

Gupta, V. K., Sureshkumar, R. & Khomami, B. 2005 Passive scalar transport in polymer drag-reduced turbulent channel flow. *AIChE J*., **51**, 1938–1950.

Hou, Y. X., Somandepalli, V. S. R. & Mungal, M. G. 2006 A technique to determine total shear stress and polymer stress profiles in drag reduced boundary layer flows. *Exps. Fluids* **40**, 589–600.

Jimenez, J. & Pinelli, A. 1999 The autonomous cycle of near wall turbulence. *J. Fluid Mech.* **398**, 335–339.

Koskie, J. E. & Tiederman, W. G. 1991a Turbulent structure and polymer drag reduction in adverse pressure gradient boundary layers. PME-FM-91-3, Office of Naval Research.

Koskie, J. E. & Tiederman, W. G. 1991b Polymer drag reduction of a zero-pressure-gradient boundary layer. *Phys. Fluids* **A3**, 2471–2473.

Latto, B. & El Reidy, K. F. 1976 Diffusion of polymer additives in a developing turbulent boundary layer. *J. Hydronaut*. **10**, 135–139.

McComb, W. D. & Rabie, L. H. 1982 Local drag reduction due to injection of polymer solution into turbulent flow in a pipe. Part 1: dependence on local polymer concentration; and Part II: laser Doppler measurements of turbulence structure. *AIChE J*. **28**, 547–565.

Min, T., Yoo, J. Y., Choi, H. & Joseph, D. D. 2003 Drag reduction by polymer additives in a turbulent channel flow. *J. Fluid Mech.* **486**, 213–238.

Oldaker, D. K. & Tiederman, W. G. 1977 Structure of the turbulent boundary layer in drag reducing pipe flow. *Phys. Fluids* **20**, 133–144.

Paschkewitz, J. S., Dimitropoulos, C. D., Hou, Y. X., Somandepalli, V. S. R., Mungal, M. G., Shaqfeh, E. S. G. & Moin, P. 2005 An experimental and numerical investigation of drag reduction in a turbulent boundary layer using a rigid rodlike polymer. *Phys. Fluids* **17**, 085101.

Petrie, H. L. & Fontaine, A. A. 1996 Comparison of turbulent boundary layer modifications with slot-injected and homogeneous drag-reducing polymer solutions, *Proc. Fluids Eng. Div. Conf. ASME* vol. 2, pp. 205–210.

Petrie, H. L., Deutsch, S., Brungart, T. A. & Fontaine, A. A. 2003 Polymer drag reduction with surface roughness in flat-plate turbulent boundary layer flow. *Exps. Fluids* **35**, 8–23.

Poreh, M. & Cermak, J . E. 1964 Study of diffusion from a line source in a turbulent boundary layer. *Intl J. Heat Mass Transfer* **7**, 1083–1095.

Purtell, L. P., Klebanoff, P. S. & Buckley, F. T. 1981 Turbulent boundary layers at low Reynolds numbers. *Phys. Fluids* **24**, 802–811.

Roach, P. E. & Brieley, D. H. 1989 The influence of a turbulent freestream on zero pressure gradient transitional boundary layer development including the condition test cases T3A and T3B. In *Numerical Simulation of Unsteady Flows and Transition to Turbulence* (ed. O. Pironneau *et al.*), Cambridge University Press.

Sibilla, S. & Baron, A. 2002 Polymer stress statistics in the near-wall turbulent flow of a drag reducing solution. *Phys. Fluids* **14**, 1123–1136.

Somandepalli, V. S. R. 2006 Combined PIV and PLIF measurements in a polymer drag reduced turbulent boundary layer. PhD thesis, Mechanical Engineering Department, Stanford University.

Terrapon, V., Dubief, Y., Moin, P., Shaqfeh, E. & Lele, S. 2004 Simulated polymer stretch in a turbulent flow using Brownian dynamics. *J. Fluid Mech.* **504**, 61–71.

Tiederman, W. G., Luchik, T. S. & Bogard, D. G. 1985 Wall layer structure and drag reduction. *J. Fluid Mech.* **156**, 419–437.

den Toonder, J., Hulsen, M., Kuiken, G. & Nieuwstadt, F. 1997 Drag reduction by polymer additives in a turbulent pipe flow: numerical and laboratory experiments. *J. Fluid Mech.* **337**, 193–231.

Vdovin, A. V. & Smol'yakov, A. V. 1978 Diffusion of polymer solutions in a turbulent boundary layer. *Zh. Prikl. Mekh. Tekh. Fiz*. **2**, 66–73 (transl. in UDC 532.526, pp. 196-201, Plenum).

Vdovin, A. V. & Smol'yakov, A. V. 1981 Turbulent diffusion of polymers in a boundary layer. *Zh. Prikl. Mekh. Tekh. Fiz*. **4**, 98–104 (transl. in UDC532.526 (1982) 526–531, Plenum).

Virk, P. S. 1975 Drag reduction fundamentals. *AIChE J*. **22**, 625–656.

Walker, D. T. & Tiederman, W. G. 1988 Turbulent structure and mass transport in a channel flow with polymer injection. *Rep.* PME-FM-22-2. Purdue University.

Walker, D. T. & Tiederman, W. G. 1989 The concentration field in a turbulent channel flow with polymer injection at the wall. *Exps. Fluids* **8**, 86–94.

Walker, D. T. & Tiederman, W. G. 1990 Turbulent structure in a channel flow with polymer injection at the wall. *J. Fluid Mech.* **218**, 377–403.

Walker, D. T., Tiederman, W. G. & Luchik, T. S. 1986 Optimization of the injection process for drag reduction additives. *Exps. Fluids* **4**, 114–120.

Warholic, M. D., Massah, H. & Hanratty, T. J. 1999 Influence of drag-reducing polymers on turbulence: effects of Reynolds number, concentration and mixing. *Exps. Fluids* **27**, 461–472.

Warholic, M. D., Heist, D. K., Katcher, M. & Hanratty, T. J. 2001 A study with particle image velocimetry of the influence of drag reducing polymers on the structure of turbulence. *Exps. Fluids* **31**, 474–483.

White, C. M., Somandepalli, V. S. R. & Mungal, M. G. 2004 The turbulence structure of drag-reduced boundary layer flow. *Exps. Fluids* **36**, 62–69.

White, C. M., Somandepalli, V. S. R., Dubief, Y. & Mungal, M. G. 2006 Dynamical contributions to the skin friction in polymer drag reduced wall-bounded turbulence. *Phys. Fluids* (submitted).

White, F. M. 1991 *Viscous Fluid Flow* 2nd edn. McGraw–Hill.

Wu, J. & Tulin, M. P. 1972 Drag reduction by ejecting additive solutions into a pure water boundary layer. *Trans. ASME* D: *J. Basic Engng* **94**, 749–755.